

Review

# Fluorescent and colorimetric sensors for anions: Highlights from 2020 to 2022



Giacomo Picci<sup>a</sup>, Riccardo Montis<sup>b</sup>, Alexander M. Gilchrist<sup>c</sup>, Philip A. Gale<sup>d,\*</sup>,  
Claudia Caltagirone<sup>a,\*</sup>

<sup>a</sup> Dipartimento di Scienze Chimiche e Geologiche, Università degli Studi di Cagliari, S.S. 554 Bivio per Sestu, 09042 Monserrato, CA, Italy

<sup>b</sup> Department of Pure and Applied Science, University of Urbino, Via della Stazione 4, I-61029 Urbino, Italy

<sup>c</sup> The University of Sydney, School of Chemistry, Sydney, NSW 2006, Australia

<sup>d</sup> University of Technology Sydney, Faculty of Science, School of Mathematical and Physical Science, Ultimo, NSW 2007, Australia

## ARTICLE INFO

### Keywords:

Supramolecular chemistry  
Anion sensing  
Fluorescence  
Optical chemosensors

## ABSTRACT

The development of colorimetric and fluorescent sensors continues apace. In this review, we highlight developments made in this area from 2020 to 2022. The review is structured by the different non-covalent interactions used to bind anions in addition to covering photoswitchable systems, excimers and molecular logic gates, and arrays for anion sensing.

## 1. Introduction

Anions play a multitude of roles in biological and industrial processes. Significant effort has been devoted to the development of colorimetric and fluorescent sensors for anionic guests. This review covers advances in this area between the years 2020 and 2022. The review is structured by the different non-covalent interactions used to bind anions in addition to covering photoswitchable systems, excimers and molecular logic gates, and arrays for anion sensing. Interesting developments over this period include the use of vesicles as filters for improving the performance of sensors and further developments of sensors that can be used within cells.

## 2. Hydrogen bond based chemosensors

Chemosensors containing urea and thiourea groups have been widely reported in the literature. These functional groups can efficiently interact with the anions via the formation of directional hydrogen bonds, and in the presence of suitable fluorophores or chromophores, the optical properties of chemosensors can be finely tuned. Recently Vega, Lara, and co-workers have reported the bis-urea, **1**, bearing two naphthalene substituents as a fluorescent ON-OFF sensor for oxoanions and acetate ( $\text{AcO}^-$ ) in particular (Fig. 1) [1]. The presence of the polyether bridge also allowed for the binding of metal ions. Upon the addition of

increasing amounts of  $\text{AcO}^-$  (as its tetrabutylammonium (TBA) salt) in  $\text{CH}_3\text{CN}:\text{dimethylsulfoxide}$  (DMSO) (9:1, v/v) to a solution of **1** ( $5.0 \times 10^{-6}$  M), caused quenching of the emission band of the system (centred at 367 nm) due to the electron transfer (eT) from the carbonyl group of the urea moiety to the naphthalene substituents in the excited state. The preferential formation of a 1:2 (1:2( $\text{AcO}^-$ )) adduct was demonstrated by DFT calculations.

Interestingly, recent literature concerning anion sensing with urea receptors has moved towards the development of novel materials. As an example, Chen and co-workers reported on the aggregation-induced emission (AIE) of urea-containing poly(phenylene ethynylene) **2** (Fig. 2) [2]. The aggregation properties of **2** were investigated in the absence and in the presence of anionic guests ( $\text{CN}^-$ ,  $\text{N}_3^-$ ,  $\text{AcO}^-$ ,  $\text{F}^-$ ,  $\text{Cl}^-$ ,  $\text{I}^-$ , and  $\text{Br}^-$ ) in dimethylformamide (DMF)/ $\text{H}_2\text{O}$  (1:1, v/v). Polymer **2** exhibited an emission band at 442 nm: upon the addition of the anion guests, a quenching of the emission was observed in all cases;  $\text{CN}^-$  also caused a remarkable red shift moving the emission band at 464 nm (Fig. 2A). To study the effect of the presence of the anionic guests on the aggregation properties of the polymer, dynamic light scattering (DLS) analysis was performed. As clear from Fig. 2B, the addition of the anion caused a disaggregation of the polymer with a decrease of the average hydrodynamic diameter ( $D_h$ ) in the presence of various anions. Given the selective fluorescence response of polymer **2** towards  $\text{CN}^-$ , the authors investigated the effect of the concentration of  $\text{CN}^-$  on the

\* Corresponding authors.

E-mail addresses: [philip.gale@uts.edu.au](mailto:philip.gale@uts.edu.au) (P.A. Gale), [ccaltagirone@unica.it](mailto:ccaltagirone@unica.it) (C. Caltagirone).

<https://doi.org/10.1016/j.ccr.2023.215561>

Received 5 October 2023; Accepted 6 November 2023

Available online 12 December 2023

0010-8545/© 2023 The Author(s). Published by Elsevier B.V. This is an open access article under the CC BY license (<http://creativecommons.org/licenses/by/4.0/>).

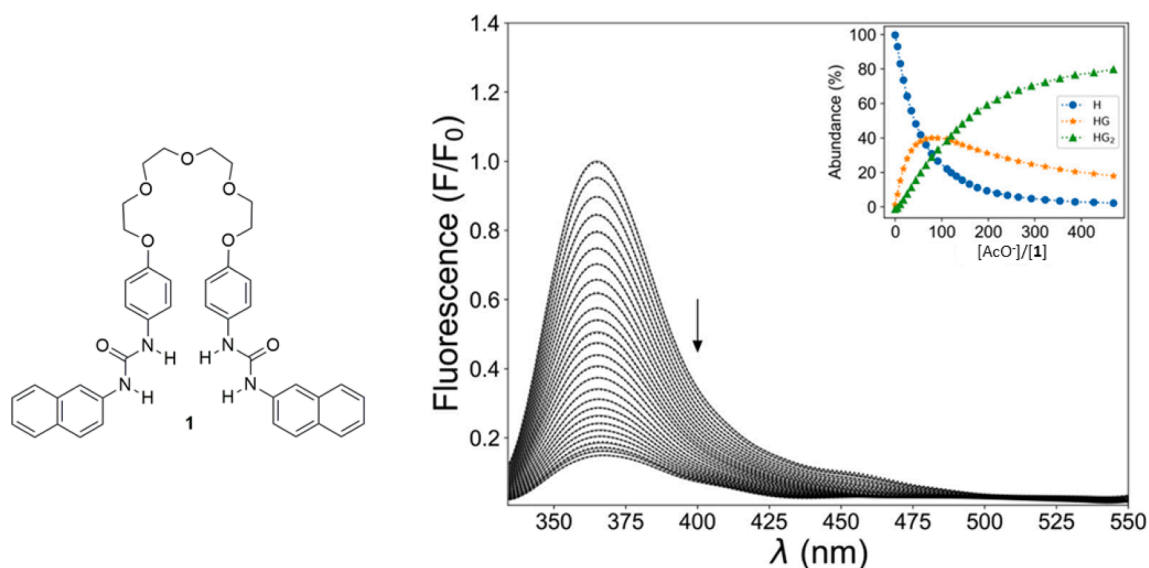


**Fig. 1.** Changes in the emission spectrum of **1** ( $5.0 \times 10^{-6}$  M) upon the addition of increasing amounts of TBAAcO ( $0\text{--}2.35 \times 10^{-3}$  M) in  $\text{CH}_3\text{CN}:\text{DMSO}$  (9:1, v/v),  $\lambda_{\text{exc}} = 298$  nm. Inset: speciation of H (**1**), HG (1:1, 1:AcO<sup>-</sup> adduct) and HG<sub>2</sub> (1:2, 1:2(AcO<sup>-</sup>) adduct). Reproduced with permission from Ref. [1]. Copyright ACS, 2022.

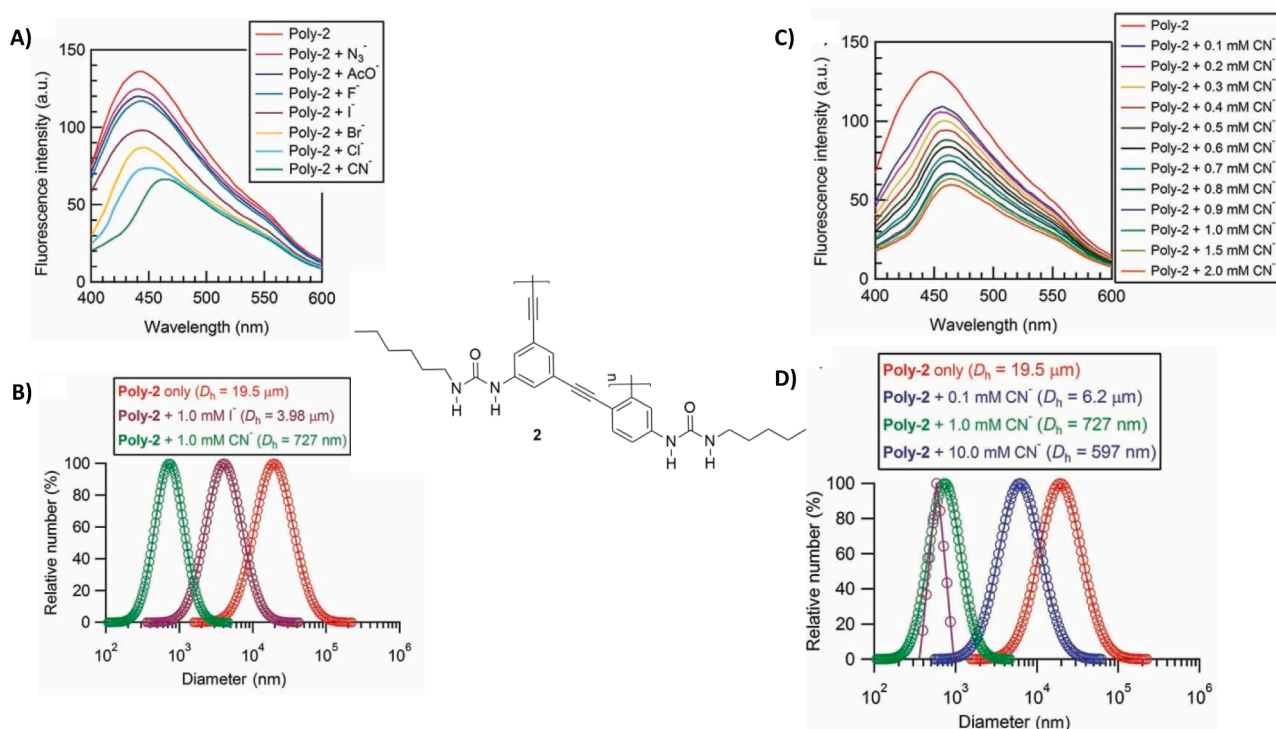


**Fig. 2.** A) Changes in the fluorescence emission of polymer **2** in  $\text{DMF}/\text{H}_2\text{O}$  (1:1, v/v) upon the addition of different anions. B) Changes in the average dynamic diameter of **2** in the presence of I<sup>-</sup> (purple) and CN<sup>-</sup> (green). C) Quenching of the fluorescence emission of polymer **2** in  $\text{DMF}/\text{H}_2\text{O}$  (1:1, v/v) upon the addition of increasing amounts of CN<sup>-</sup>. D) Changes in the average dynamic diameter of **2** in the presence of increasing amounts of CN<sup>-</sup>. Copyright Taylor and Francis 2021. Reproduced with permission from Ref. [2].

aggregate's dimensions. A net decrease in the dimension of the particles was observed with the concomitant fluorescence quenching illustrating the AIE properties of the system.

By dispersing polyvinyl *N*-(4-(4-nitrophenylazo)phenyl)-*N'*-methylthiourea into polymethylmethacrylate (PMMA) fibres, Kato and co-workers were able to obtain a polymer for the sensing of hydrophilic anions in protic solvents [3]. Methanolic solutions of hydrophilic anions such as Cl<sup>-</sup>, AcO<sup>-</sup>, and H<sub>2</sub>PO<sub>4</sub><sup>-</sup> could penetrate the nanofibers of the

material, causing a change in the intensity of the diffuse-reflection absorption spectrum of the polymer and a red-shift of the absorption band due to the formation hydrogen bonding interactions between the anionic guests and the thiourea moieties. It was also demonstrated that the polymers response to the tested anions was dependent on the thickness of the fibres (the thinner the fibres, the smallest was the response).

A novel approach for fluoride sensing has been introduced by Torres, Brovotto, Veiga, and co-workers, who reported a urea-based imprinting

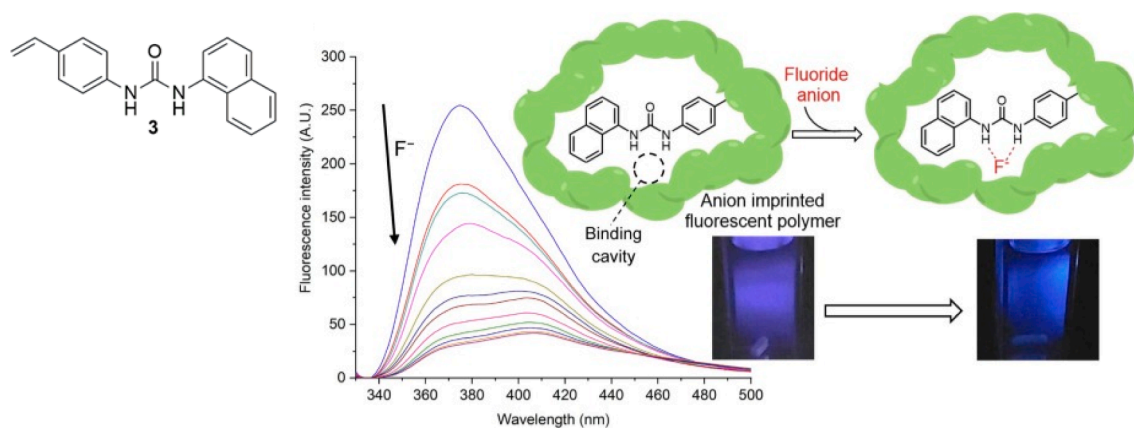


**Fig. 3.** Fluorescence quenching caused by fluoride in DMSO in the imprinted polymer based on receptor **3** ( $\lambda_{\text{exc}} = 319$  nm). Reproduced with permission from Ref. [4]. Copyright Elsevier 2022.

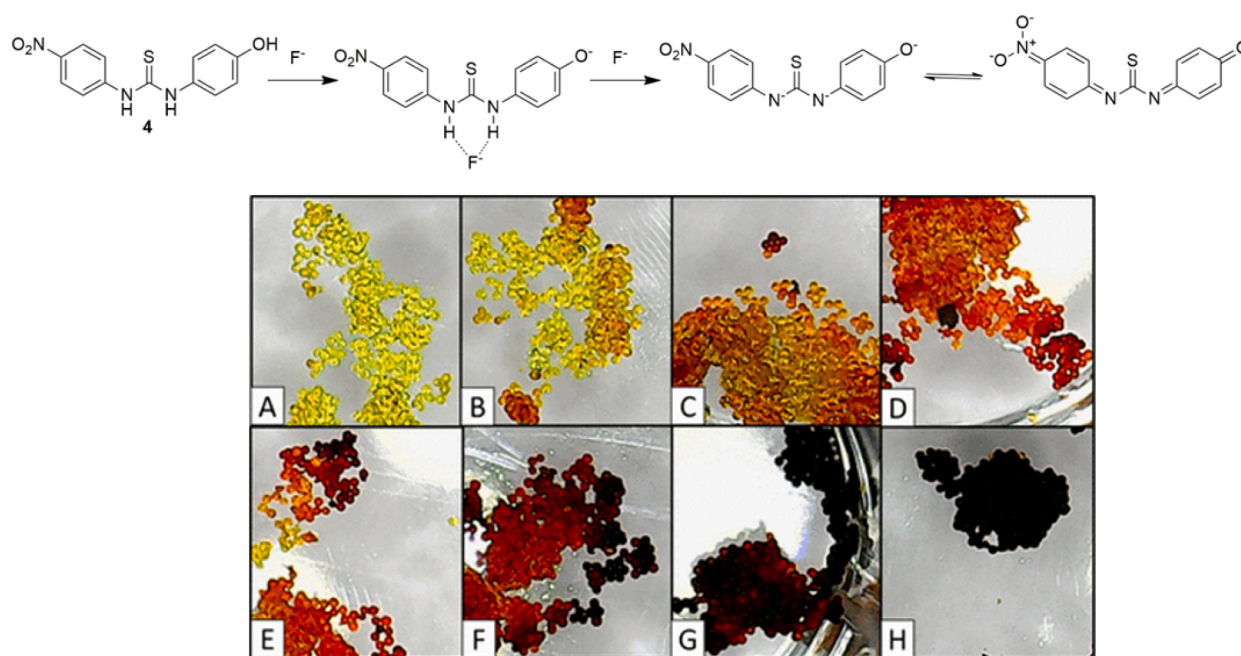


**Fig. 4.** 1) Proposed scheme for the binding/deprotonation process of fluoride by thiourea **4** and 2) the colorimetric response of **4** towards increasing concentrations of  $\text{F}^-$  (added as TBAF) supported by Tentagel resin in  $\text{H}_2\text{O}$ : A) resin functionalised with **4**, B) TBAF (0.2 mM), C) TBAF (0.4 mM), D) TBAF (0.6 mM), E) TBAF (0.8 mM), F) TBAF (1 mM), G) TBAF (2.5 mM), H) TBAF (5 mM). Reproduced with permission from Ref. [5]. Copyright ACS 2021.

polymer capable of sensing the presence of fluoride anions [4]. In order to enhance the sensing properties of the fluorescent urea **3** (Fig. 3), the authors prepared a polymeric optical sensor by reacting compound **3** with ethylene glycol dimethacrylate (EDMA) as cross-linking agent and 2,2'-azobis(2-methylpropanitrile) (AIBN) in the presence of  $\text{F}^-$  as the TBA salt. Removal of the anion led to the novel polymeric materials with a specific binding pocket for the anion. Upon the addition of  $\text{F}^-$  to a solution of the polymer in DMSO, a quenching of the emission band at 374 nm was observed (Fig. 3). Compared to the free receptor, the sensitivity towards fluoride improved in the polymer (LOD = 18.3  $\mu\text{M}$  in **3** and 11.3  $\mu\text{M}$  in the polymer). Moreover, the interference of the other anions, especially  $\text{H}_2\text{PO}_4^-$ , is negligible, with 70 % of  $\text{F}^-$  entrapped by the polymeric matrix vs 4.8 % of  $\text{H}_2\text{PO}_4^-$ .

Thiourea **4** bearing a phenol group was studied in a DMSO solution with different anions [5]. It was demonstrated that in DMSO solution  $\text{AcO}^-$ ,  $\text{H}_2\text{PO}_4^-$ , and  $\text{F}^-$  anions deprotonated the phenol OH and subsequently the thiourea NHs causing the solution to change colour. Thiourea **4** was linked to Tentagel resin as a solid support, and the

functionalised resin could detect the presence of fluoride even in 100 % aqueous solution (Fig. 4).

Interestingly, although the solid support allowed for sensing in 100 % water, the sensitivity of the system decreased when compared to the DMSO solution, presumably due to enhanced competition for the formation of hydrogen bonds between the thiourea NH groups, fluoride anions and the oxygen atoms of the polyethylene groups of the PEG at the surface of the resin.

Busschaert and co-workers have demonstrated an innovative method to enhance the selectivity of sensors called the transporter-liposome-fluorophore (TLF) approach [6]. As shown in Fig. 5A, this method is based on the encapsulation of a non-selective fluorophore inside liposomes and the use of non-selective small molecule transporters to enhance the fluorophore response. Only the analytes that are transported inside the vesicles and can give an optical response can be sensed. Lucigenin was chosen as fluorophore and 1,3-diphenylurea as anionophore. Lucigenin (1 mM) was encapsulated inside egg phosphatidylcholine (EggPC) unilamellar vesicles (100 nm) containing  $\text{NaNO}_3$  and

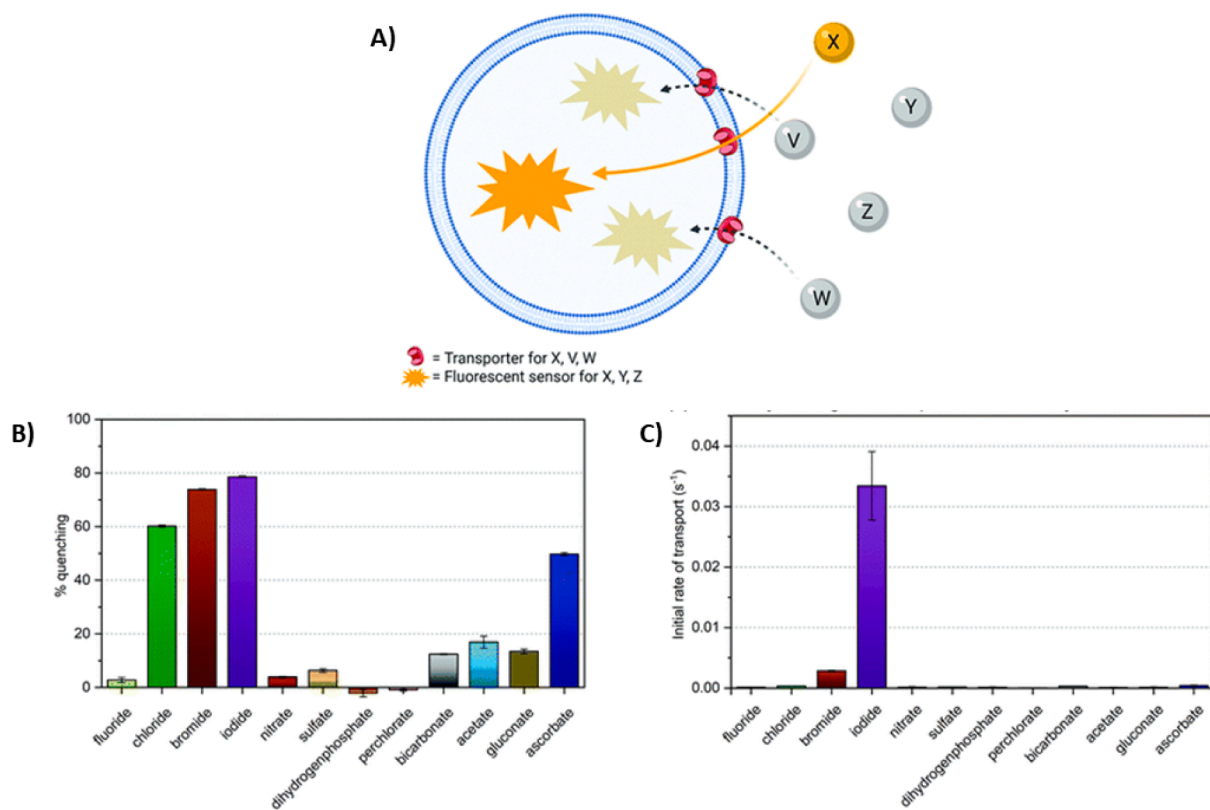


**Fig. 5.** A) Scheme describing the TLF approach; B) percentage of quenching of free lucigenin upon addition of various anions as their sodium salts at 16.4 mM; C) TLF approach response evaluated considering the initial rate of transport by different anions as their sodium salts at 25 mM. Adapted with permission from Ref. [6]. Copyright RSC 2020.

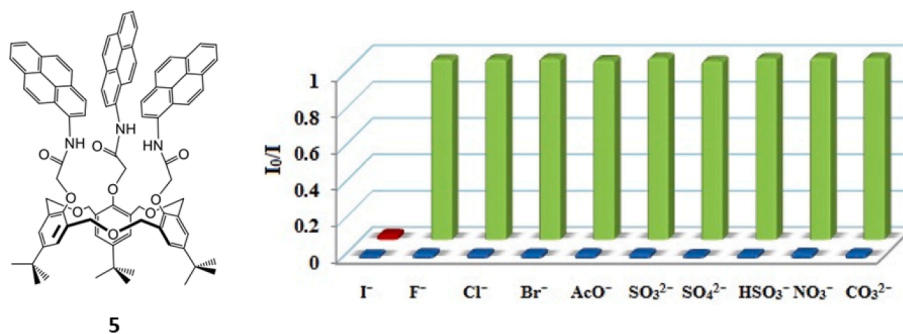


**Fig. 6.** Competition experiments conducted on **5** in THF/H<sub>2</sub>O (7:3, v/v) at pH = 7.0 buffered with Tris-HCl. The green bar represents the fluorescence intensity ( $I_0/I$ ) response at 458 nm of **5** in the presence of 100 equivs. of each tested anion. The blue bar represents the  $I_0/I$  response at 458 nm of **5** in the presence of 100 equivs. of I<sup>-</sup> and 100 equivs. of each tested anion. The red bar represents the response of **5** in the presence of I<sup>-</sup> and all the other anions. Reproduced with permission from Ref. [13]. Copyright Elsevier 2020.

buffered to pH 7.4 with 4-(2-hydroxyethyl)-1-piperazineethanesulfonic acid (HEPES), while the vesicles were suspended in a solution of NaNO<sub>3</sub> (22 mM), NaI (25 mM), and HEPES at pH 7.4. A DMF solution of the anionophore was added, and the transport was monitored for 5 min following the quenching of the lucigenin. The experiment was performed in the presence of various anions (F<sup>-</sup>, Cl<sup>-</sup>, Br<sup>-</sup>, NO<sub>3</sub><sup>-</sup>, SO<sub>4</sub><sup>2-</sup>, H<sub>2</sub>PO<sub>4</sub><sup>-</sup>, ClO<sub>4</sub><sup>-</sup>, HCO<sub>3</sub><sup>-</sup>, AcO<sup>-</sup>, gluconate, and ascorbate) and as shown in Fig. 5B and C a great enhancement of the selectivity towards I<sup>-</sup> was observed in the TLF approach when compared to the free lucigenin.

Amide-based chemosensors have continued to attract the attention of researchers [7–12]. The C<sub>3v</sub> symmetry hexahomotrioxacalix[3]arene **5** functionalised with three pyrene moieties as the active fluorescent units has been reported by Zhang, Yamato, and co-workers (Fig. 6) [13]. Upon excitation of **5** at 346 nm, a selective quenching of the fluorescence band

at 484 nm was observed in the presence of I<sup>-</sup> with respect to other anions (F<sup>-</sup>, Cl<sup>-</sup>, Br<sup>-</sup>, AcO<sup>-</sup>, SO<sub>3</sub><sup>2-</sup>, SO<sub>4</sub><sup>2-</sup>, HSO<sub>3</sub><sup>-</sup>, NO<sub>3</sub><sup>-</sup>, and CO<sub>3</sub><sup>2-</sup> added as sodium salts) in tetrahydrofuran (THF)/H<sub>2</sub>O (7:3, v/v) at pH = 7.0 buffered with Tris-HCl. Competition studies demonstrated that the other anions tested did not cause interference with I<sup>-</sup> (Fig. 6). The chemosensor works in I<sup>-</sup> concentrations ranging from 0 to 200 μM with a LOD of 164 nM. Using <sup>1</sup>H NMR titrations, the authors demonstrated that a change in the conformation of the macrocycle occurs in the presence of I<sup>-</sup> which interacts with the three amide moieties via the formation of hydrogen bonding interactions. The authors explain the observed fluorescence quenching of **5** is due to the formation of the H-bonds in tandem with the heavy atom effect that causes an increase in the population of the non-emissive triplet state.

The selective detection of CN<sup>-</sup> in 100 % H<sub>2</sub>O by the acetamide

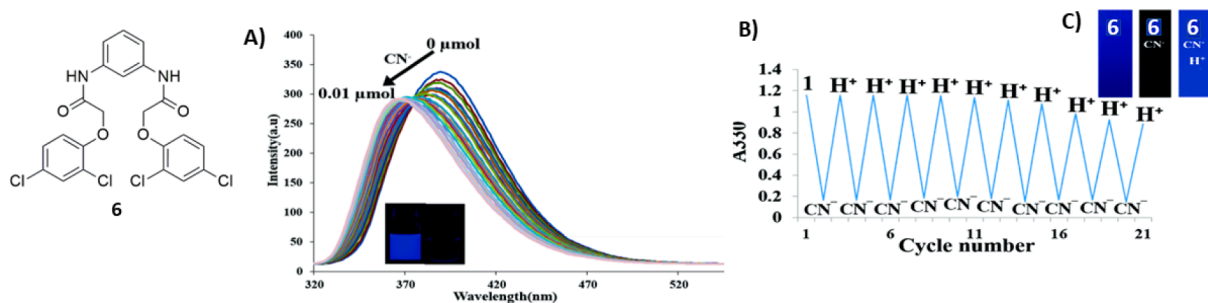


Fig. 7. The chemical structure of **6**, and A) the fluorescence titration of **6** in the presence of  $\text{CN}^-$  and a picture showing the changes in the emission under UV light.

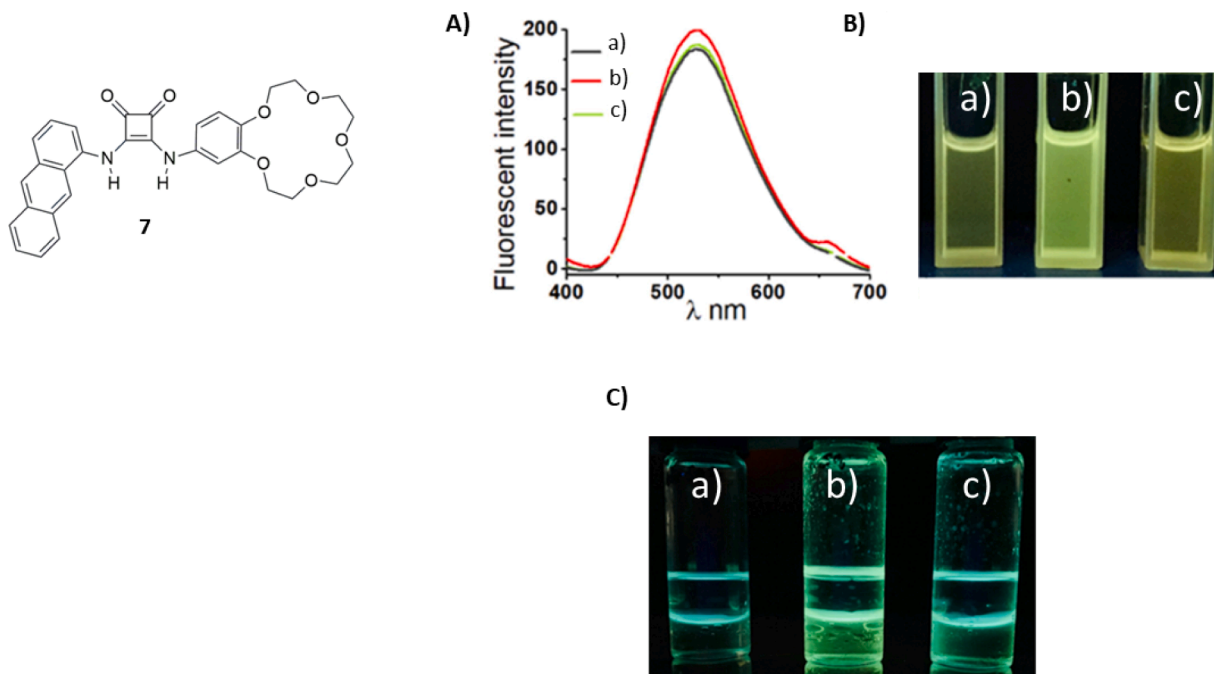


Fig. 8. A) Fluorescence spectra ( $\lambda_{\text{exc}} = 327 \text{ nm}$ ) of **7** a), **7** + 5 equivs. of  $(\text{TBA})_2\text{SO}_4$  b), **7** + 5 equivs. of  $\text{TBACl}$  c) in  $\text{CH}_3\text{CN}/\text{H}_2\text{O}$  (9:1, v/v). B) Pictures of **7** a), **7** + 5 equivs. of  $(\text{TBA})_2\text{SO}_4$  b), **7** + 5 equivs. of  $\text{TBACl}$  c) in  $\text{CH}_3\text{CN}/\text{H}_2\text{O}$  (9:1, v/v) under UV light (254 nm). C) Pictures of a) a solution of **7** in  $\text{CHCl}_3$  in contact with an aqueous solution, b) after extraction of an aqueous solution of  $\text{K}_2\text{SO}_4$ , and c) after extraction of an aqueous solution of  $\text{KCl}$ . Reproduced from Ref. [21]. Copyright MDPI 2021.

derivative **6** was reported by Darabi and co-workers (Fig. 7) [14]. When dissolved in an organic solvent, such as DMF, **6** showed a weak emission at 359 nm ( $\Phi = 0.015$ ); however, upon the addition of increasing amounts of water, an intense fluorescence emission at 389 nm appeared ( $\Phi = 0.1$ ). This is due to AIE as **6** can self-assemble, forming intramolecular H-bonds and  $\pi$ - $\pi$  stacking in the presence of water. In a 100 % aqueous solution at pH = 7.4 upon the formation of a 1:1 adduct ( $K_a = 4 \times 10^8$ ) with  $\text{CN}^-$  (as the sodium salt), the emission of **6** is blue shifted to 359 nm, suggesting that the presence of  $\text{CN}^-$  disassembles the system (Fig. 7A). All the other tested anions ( $\text{Br}^-$ ,  $\text{Cl}^-$ ,  $\text{F}^-$ ,  $\text{I}^-$ ,  $\text{SCN}^-$ ,  $\text{S}^{2-}$ ,  $\text{SO}_4^{2-}$ ,  $\text{SO}_3^{2-}$ ,  $\text{S}_2\text{O}_3^{2-}$ ,  $\text{S}_2\text{O}_4^{2-}$ ,  $\text{S}_2\text{O}_5^{2-}$ ,  $\text{ClO}_3^-$ ,  $\text{ClO}_4^-$ ,  $\text{IO}_3^-$ ,  $\text{IO}_4^-$ ,  $\text{CH}_3\text{COO}^-$ ,  $\text{BrO}_3^-$ ,  $\text{HSO}_4^-$ ,  $\text{MoO}_4^{2-}$ ,  $\text{H}_2\text{PO}_4^-$ ,  $\text{NO}_3^-$ , and  $\text{NO}_2^-$ ) resulted in no observed changes. A LOD of 8.2 nM was calculated for  $\text{CN}^-$ . The changes in the fluorescence emission caused by  $\text{CN}^-$  are reversible upon the addition of  $\text{HCl}$ , the original emission is restored both in solution and in solid-state on strip test (Fig. 7B–C). This interesting system is also able to detect  $\text{CN}^-$  extracted from apricots, peaches, and bitter almond seeds.

Compared to analogous ureas and amides, it has been demonstrated that the use of squaramide-based receptors offers several advantages in terms of anion binding efficiency [15–20].

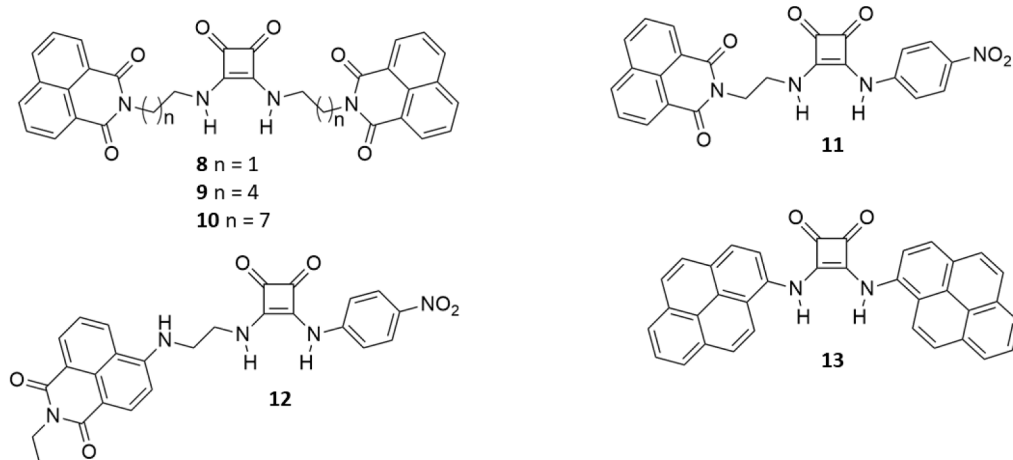
The fluorescent heteroditopic receptor **7**, reported by Romański and

co-workers, is able to extract sulfate salts and detect them via fluorescence emission (Fig. 8) [21]. The squaramide portion of the molecule interacts with the  $\text{SO}_4^{2-}$  anions, the benzo-18-crown-6 interacts with the metal cation, while the anthracene moiety acts as the fluorescent unit. As shown in Fig. 8A and B, in a solution of  $\text{CH}_3\text{CN}/\text{H}_2\text{O}$  (99:1, v/v), the fluorescence emission of **7** increased upon the addition of 5 equivs. of  $(\text{TBA})_2\text{SO}_4$ , probably because of an exchange between the water molecules and the anion within the binding sites of the chemosensor. Upon the addition of  $\text{TBACl}$ , the fluorescence did not appreciably change. Similar changes were observed in  $\text{CHCl}_3$ , and this gave the possibility to develop a two-phase fluorescent sensor as the system can selectively extract  $\text{K}_2\text{SO}_4$  from water and change its fluorescent emission (Fig. 8C).

Elmes and co-workers have very recently described the self-aggregation behaviour of naphthalimido-squaramides **8–10**, which did not show any specific sensitivity towards anions, although anion binding selectivity was observed towards  $\text{AcO}^-$  in  $\text{DMSO}-d_6$  during  $^1\text{H}$  NMR titrations at 298 K [22]. The authors showed that the non-symmetric naphthalimido-squaramides **11** and **12** also self-aggregate and change colour in solution upon deprotonation in the presence of basic anions such as  $\text{F}^-$ ,  $\text{AcO}^-$ ,  $\text{SO}_4^{2-}$ , and  $\text{H}_2\text{PO}_4^-$  [23].

Caltagirone, Picci, and co-workers have shown that the  $\text{Cu}(\text{II})$

complex of bis-pyrenyl-squaramide **13** is capable of switch-on fluorescence sensing towards basic anions ( $\text{OH}^-$ ,  $\text{CN}^-$ , and  $\text{F}^-$  as their TBA salts) in  $\text{CH}_3\text{CN}$  via deprotonation of the squaramide NHs [24].



Various research groups have also reported imidazole-based chemosensors in the last few years [25–31]. Misra and co-workers have described the sensing properties based on the intramolecular charge transfer mechanism towards  $\text{CN}^-$  and  $\text{F}^-$  of the imidazole derivative **14** (Fig. 8) [32]. Chemosensor **14** showed a solvatochromic behaviour with a bathochromic shift of the emission with the increase of the polarity of the solvent and a tendency to aggregate in 1,4-dioxane with a disaggregation effect due to the presence of water. In the presence of basic anions such as  $\text{CN}^-$  and  $\text{F}^-$  in a 1,4-dioxane solution, dramatic changes in the absorption and emission properties of **14** were observed. The absorption band of the free chemosensor at 416 nm was red-shifted to 538 nm upon the addition of  $\text{F}^-$  and further blue-shifted to 122 nm in the case of  $\text{CN}^-$  (Fig. 9A) with the colorimetric changes being observable by the naked eye.

The emission band at 548 nm of the free **14** (arising from excitation at 416 nm) was quenched and blue-shifted (at 488 nm) upon the addition of 7 equivs. of  $\text{CN}^-$ , while a simple quenching was observed when titrating **14** with an increasing concentration of fluoride. Proton-NMR titrations in  $\text{DMSO}-d_6$  were used to elucidate the interaction between the chemosensor and the tested anions, which is an acid-base interaction with  $\text{F}^-$  with deprotonation of the imidazole N–H and a H-bond interaction along with a nucleophilic Michael addition at the lactone moiety of the coumarin fragment of **14** with  $\text{CN}^-$ .

### 3. Halogen-bond based chemosensors

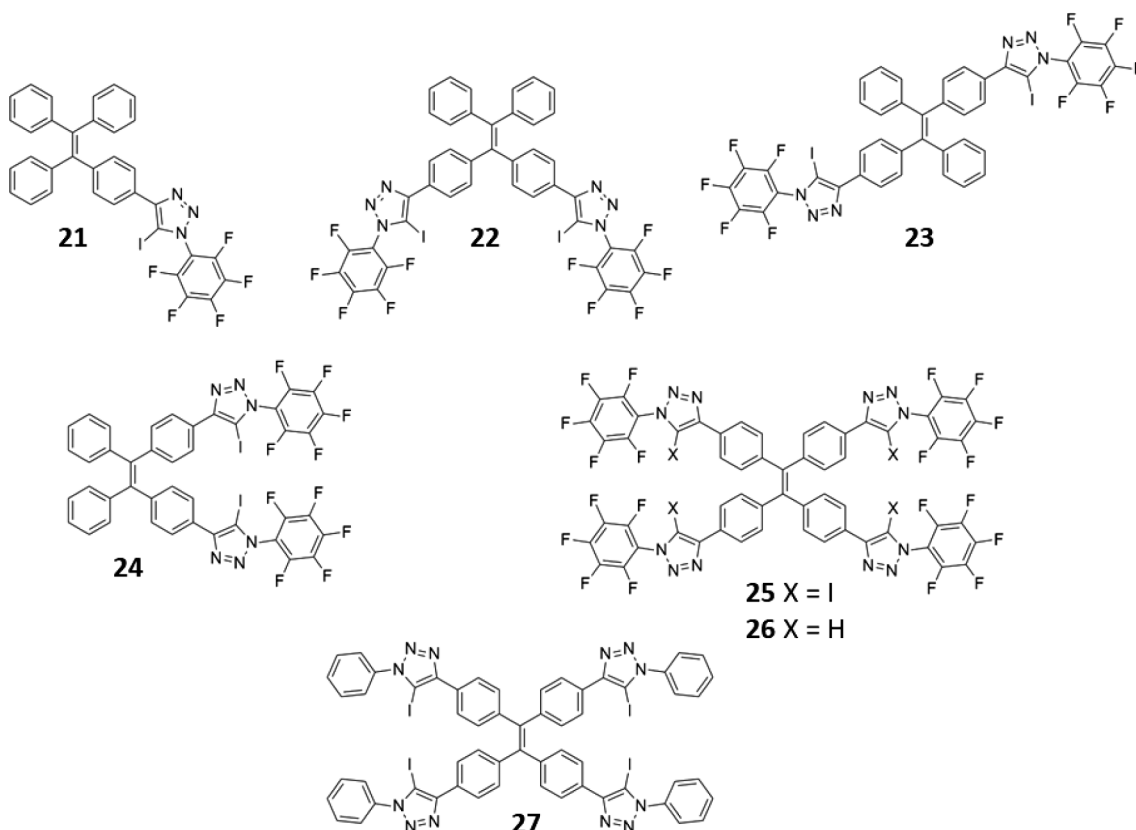
Due to their directionality and strength, halogen bonds (XBs) [33] represent another important intermolecular interaction for the design of supramolecular systems [34]. According to the recommendation of IUPAC [35], a halogen bond “occurs when there is evidence of a net attractive interaction between an electrophilic region associated with a halogen atom in a molecular entity and a nucleophilic region in another, or

the same, molecular entity”. In other words, a halogen bond is a highly directional and attractive interaction occurring between an electron-deficient halogen atom and a nucleophile or a Lewis base. Amongst the variety of electron-rich systems, anions represent good candidates to

interact with electron-deficient halogen atoms. Accordingly, over the past few years, halogen bonding has become a promising tool for the design of anion receptors and probes [36]. Recent work focused on the design of probes based on iodo-triazole derivatives [37–40].

In a recent article [39], Beer and co-workers described three new probes containing pyridine (**15**), pyridinium (**16**) or a secondary amine (**17**) spacers, functionalized with coumarin fluorophores decorated with hydrophilic triethylene glycol (TEG) substituents and incorporated into a XB bis-iodotriazole donor-site (Fig. 10). Analogous hydrogen bonding-based receptors (**18–20**) were also synthesized and their properties compared to compounds **15–17** (Fig. 10). The sensing ability of the receptors towards  $\text{HS}^-$  and halides were investigated by fluorescence spectroscopy in buffered aqueous solutions (HEPES buffer at pH 7.4). Among the three XB-based receptors, **15** exhibited the highest selectivity for  $\text{HS}^-$ , behaving as a supramolecular probe for  $\text{HS}^-$  over the halides. When excited at 342 nm, **15** showed a significant quench of its fluorescence emission (60 %) only in the presence of  $\text{HS}^-$  (Fig. 10A), while no variation of the emission intensity was observed in the presence of halides ( $\text{Cl}^-$ ,  $\text{Br}^-$ , and  $\text{I}^-$ , Fig. 10B). In the case of **16**, the addition of an increasing amount of  $\text{HS}^-$  resulted in quenching of the fluorescence emission of approximately 45 %. In the presence of halogens, the receptor exhibited a response only upon the addition of  $\text{Br}^-$  and  $\text{I}^-$ . Receptor **17**, under the experimental conditions used for the titration experiments, existed mainly in its protonated form  $17\text{H}^+$ . Upon addition of the target anion species,  $17\text{H}^+$  responded only in the presence of  $\text{HS}^-$  and  $\text{I}^-$ . Interestingly, compared to their XB-based analogues, the HB-based probes **18–20** showed no detection ability towards the target anions. These results were also confirmed by density functional theory (DFT) and molecular dynamics simulations.

A recent article by Docker and Hang et al. [38] reported a family of probes (**21–27**) for anion detection based on tetraphenylethene (TPE) derivatives bearing iodo-triazole halogen bond donors.



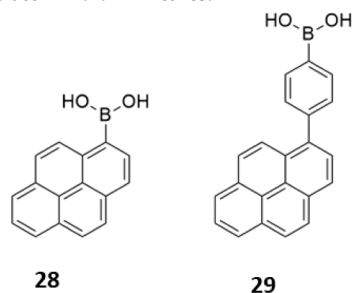
The binding ability of **21–27** towards halides was investigated using  $^1\text{H}$  NMR titration techniques in THF- $d_8$  at 298 K. The different structures of **21–27** result in different binding modes and stoichiometries. With compounds **22** and **23**, the two iodotriazole donors are too far apart to allow for chelation in a bidentate fashion. However, in the case of **24**, the two iodotriazole donors cooperate in the binding process. In particular, the differences in the anion binding properties observed for the two *E* and *Z* derivatives **23** and **24** prompted investigations on the possibility that the two isomers can be interconverted by light, acting as photo-switchable anion receptors. The presence of additional XB donors in compounds **22–27** enables higher binding stoichiometries. However, depending on the geometrical features of the binding site, the complexation with higher stoichiometry can be considerably weaker with respect to the formation of the 1:1 complex. This is the case with **24**, in which, due to the proximity of the two iodotriazole donors, the formation of the 1:2 complex shows negative cooperativity, presumably due to anion-anion repulsion. Similar behavior is observed for the tetradentate receptors **25** and **26**, while HB-based bi-dentate receptor **27** shows weak binding properties. The ability of **21–27** to detect anionic species was also investigated. The results of the fluorescence titration experiments of **21–27** in the presence of increasing amounts of halides show a strong response only in the case of the perfluoro-tetradentate **25**, which exhibits a three-fold increase of the emission band at 520 nm accompanied by a blue-shift ( $\approx 20$  nm) after the addition of 10 equiv. of  $\text{Cl}^-$  (Fig. 11A). This response is ascribed to an AIE mechanism. Single-crystal X-ray diffraction and DLS measurements confirm the tendency of **25** to aggregate in the presence of  $\text{Cl}^-$  (Fig. 11B and C). DLS measurements revealed that in the absence of  $\text{Cl}^-$  anions, **25** does not tend to form aggregates, while the addition of one equivalent of  $\text{Cl}^-$  induces the formation of aggregates with a size of approximately 100 nm (Fig. 11B).

#### 4. Boron-based chemosensors

Several boron-based chemosensors for anions have been developed recently. With the exception of systems bearing BODIPY dyes, where the boron centre is not directly involved in the interaction with the anion, there are some examples that utilise boron-based functional groups to bind anions, transducing the binding event into a colorimetric or fluorescent response. The sensing mechanism involves the addition of the nucleophilic anion (usually  $\text{F}^-$  or  $\text{CN}^-$ ) to the boron Lewis acid, with the consequent change of its geometry (from trigonal planar to tetrahedral) and electronic structure, causing changes in the photophysical properties, including absorption and emission. Among boron-based sensors, boronic acid derivatives, due to their synthetic versatility and low toxicity [41], have been extensively applied for anion sensing. Recognition of anions occurs either by exploiting the Lewis acidity of the boron centre through a direct  $\text{B-A}^-$  coordination or, in a few cases, via hydrogen bonding with the  $\text{B(OH)}_2$ .

Minami, Liu et al. [42] have recently described a fluorescent chemosensor array based on two pyrenylboronic acid derivatives (**28** and **29**) for the simultaneous discrimination of  $\text{AcO}^-$ , oxalate ( $\text{C}_2\text{O}_4^{2-}$ ), malonate ( $\text{C}_4\text{H}_2\text{O}_4^{2-}$ ), citrate ( $\text{C}_6\text{H}_5\text{O}_7^{3-}$ ),  $\text{F}^-$ , dihydrogen phosphate,  $\text{H}_2\text{PO}_4^-$ , and pyrophosphate ( $\text{HP}_2\text{O}_7^{3-}$ ). The ability of **28** and **29** to recognize the analytes was investigated by fluorescence titrations and electrospray ionization mass spectrometry (ESI-MS). Depending on the analytes, **28** and **29** responded by an OFF-ON and ON-OFF fluorescence response due to photoinduced electron transfer (PET) between the fluorophore and the boron atom, originating from anion recognition. The binding constants,  $K = 4.2 \times 10^8$  and  $1.0 \times 10^8 \text{ M}^{-1}$  were obtained for **28** and **29**, respectively. The two pyrenylboronic acid derivatives were tested as an array for the qualitative and semi-quantitative discrimination of multiple anions using a linear discriminant analysis (LDA). The array allowed the successful discrimination of seven types of anions with

100 % accuracy and the quantitative detection of oxalate, malonate, and citrate in 1:1:1 mixtures.



A recent article by Liu et al. [43] reported a BODIPY derivative bearing a pinacol boronate group (**30**) for the selective detection of  $F^-$  anions in aqueous solutions (Fig. 12A). The interaction of **30** with  $F^-$  anions caused a slight blue shift of the absorption band at 630 nm (Fig. 12B, top) and a turn-on fluorescence response at 677 nm (Fig. 12B, bottom), which proved to be stable in the pH range 3–9.

Furthermore, **30** exhibited high selectivity toward fluoride ions in the presence of other reactive cations and anions. The mechanism of recognition proposed (Fig. 12A) involves the coordination of the  $F^-$  anion by the  $sp^2$  boron, causing a change from the trigonal planar to the tetrahedral geometry, as confirmed by  $^{11}B$  NMR. Compound **30** was also tested for the detection of  $F^-$  in real water samples and in-vivo fluorescence bioimaging of  $F^-$  anions (Fig. 12C), opening the possibility of applying this system in environmental and biological samples.

The use of boronic acid derivatives to sense anions via hydrogen bonding has been recently investigated, both experimentally and computationally. Yatsimirsky and co-workers reported on the sensing properties of an anthracene appended *o*-aminomethylphenylboronic acid (**31**) towards 20 organic and inorganic anions [44]. In this case, depending on the anion species investigated, the boronic acid can interact via hydrogen bonding or directly coordinate with the anion. In the presence of fluoride anions, the Lewis acidic behavior of the  $B(OH)_2$  is favoured, as evidenced by  $^{11}B$  NMR data, that are consistent with the formation of a tetrahedral Lewis-type adduct. On the other hand, in the presence of carboxylate, phosphate and sulfate anions, the boronic acid group interacts with them by hydrogen bonding (Fig. 13). In most cases, the recognition process involves a turn-OFF fluorescence response attributed to the enhanced PET. The aminomethyl group in **31** is involved in an intramolecular hydrogen bond with the  $B(OH)_2$ . This interaction blocks the quench of the fluorescence generally observed in the case of derivatives featuring the aminomethyl group attached to anthracene and ascribed to the PET mechanism. The interaction between the boronic acid and the anion competes with the intramolecular interaction with the methyl amine group, restoring the PET-induced quench of the fluorescence.

Interestingly, in the presence of monoanions of dicarboxylic acids, the quenching of the fluorescence decreases dramatically, resulting in an opposite turn-on effect. This was explained as the result of a decrease in PET due to the formation of a  $COOH \cdots N$  hydrogen bond between the non-dissociated COOH group of the dicarboxylic acid and the aminomethyl moiety. This effect was particularly marked in the presence of the malonic acid monoanion, opening the possibility of selective detection of this species among other anions.

Boronic acid derivatives have also been employed for the design of boron-containing polymers as emerging chemosensors. Brantley and colleagues [45] developed a boron-based polymer obtained by esterification of polyvinyl alcohol with aryl boronic acids. Through UV–Vis and spectrofluorimetric titrations showed an optical response in the presence of borophilic anions such as  $OH^-$ ,  $F^-$ , and  $CN^-$ . Further DFT calculations at the B3LYP2/def2-SVP3 level of theory suggest that the anion binding process combines the Lewis acidity of B(III) through a direct  $B-A^-$  coordination and the hydrogen bond character of the other OH groups in the polymeric chain.

Triarylboranes represent another class of tri-coordinated boron derivatives that have found an application for the detection of small anionic species, such as  $F^-$  and  $CN^-$ . Qi et al. have recently reported an interesting example of an organoboron derivative with a multiple resonance (MR) effect (**32**) for the selective detection of fluoride anions (Fig. 14A) [46]. This type of fluorophore possesses useful properties, such as narrow-band emission, high fluorescence quantum yields and good chemical and thermal stability, making them the ideal candidates for several applications, including organic light-emitting diode (OLED) applications. The photophysical properties of **32** were investigated by UV–Vis absorption and fluorescence spectroscopy in THF at room temperature (298 K). Chemosensor **32** exhibited weak absorption bands between 282 nm and 368 nm and an intense band at 467 nm. A sharp and narrow emission band at 485 nm and a blue-green fluorescence was also observed. The photoluminescence quantum yield (PLQY) was 90 %. The system also exhibited excellent thermal and photochemical stability. The anion binding properties of **32** were investigated by UV–Vis and fluorescence spectroscopy in THF solutions (Fig. 14B and C). In the presence of incremental amounts of TBAF, an increase in the intensity of the emission at 282 nm and 368 nm was observed, with a concomitant decrease in the intensity of the absorption bands at 322 nm and 466 nm. Upon the progressive addition of TBAF, the emission band at 483 nm decreased dramatically. The calculated LOD was  $7.2 \times 10^{-11}$  mol  $L^{-1}$ . The quenching of the fluorescence was ascribed to the formation of the  $B-F^-$  adduct, obtained through the occupation of the empty  $p_z$  orbital of the boron center by the anionic species, destructing the MR structure of **32**. The authors used DFT calculations to confirm the disruption of the MR structure promoted by the formation of the  $B-F^-$  adduct ( $32 \cdot F^-$ ).

The crystal structure of both **32** and the  $B-F^-$  adduct were obtained by single-crystal X-ray diffraction (Fig. 14D and E). While the structure of **32** shows a trigonal planar geometry of the boron center, the  $B-F^-$  adduct clearly showed a tetra-coordinated boron center, though this is unusually bound to an oxygen atom located between the boron and the aromatic ring. This observation was explained as the result of an oxidation process that occurred during the crystallization experiment. The formation of a tetra-coordinated  $B-F^-$  adduct was further confirmed by  $^{11}B$  NMR titration experiments in THF. The results show the appearance of new signals at  $-152$  and  $11.5$  ppm, confirming the formation of a 1:1 $B-F^-$  adduct after the addition of 1 equiv. of TBAF. The calculated binding constant for the  $B-F^-$  adduct was  $K_a = 1.16 \times 10^5$   $M^{-1}$ . The 1:1 stoichiometry was also confirmed by a job plot. The formation of the  $B-F^-$  adduct was also investigated in the presence of interfering anions, such as  $Cl^-$ ,  $Br^-$ ,  $I^-$ ,  $NO_3^-$ ,  $ClO_4^-$ ,  $BF_4^-$ ,  $PF_6^-$ ,  $AcO^-$ , and  $H_2PO_4^-$ . The results suggest that **32** only exhibits remarkable fluorescence changes in the presence of  $F^-$ , while the addition of the other anions resulted in no significant changes.

Recent work has also focused on the development of triarylborane-based donor–acceptor (D–A) conjugates with improved optical properties [47–50]. Raveendran et al. investigated the influence of additional donors and acceptor groups on the optical properties and anion sensing of triarylborane–triarylamine-based donor–acceptor conjugates [51]. For this purpose, the electron-donating 4-ethynyl-*N,N*-dimethylaniline group and the electron-withdrawing 4-ethynylbenzotrile group were introduced as an additional donor (**33**) and acceptor (**34**) on the triphenylamine unit and their properties compared to the neutral derivative (**35**, Fig. 15). The photophysical properties of **33–35** were investigated in different solvents. In  $CH_2Cl_2$ , the three derivatives showed two absorption bands in the region  $\sim 260$  nm and  $\sim 390$  nm, with differences that can be ascribed to the different nature of the substituents (Fig. 15A). With respect to the reference parent compound **35**, **33** and **34** showed, respectively, a red-shift and a blue-shift of the bands attributed to intramolecular charge transfer (ICT). When excited in the region 350–425 nm, analogous shifts were observed in the emission spectra. Furthermore, **35** and **34** produced a single emission band (at  $\sim 470$  nm for **35** and  $\sim 440$  nm for **34**), while **33** exhibited two emission bands, the local excited emission band (430 nm) and the ICT

band (515 nm). Increasing the solvent polarity caused a bathochromic shift in the emission spectra of the three compounds, with an effect more pronounced for **33**. The overall results suggest that the ICT band is predominant in **33** due to the presence of the donor moieties (NMe<sub>2</sub>) and less important in **34** due to the presence of different acceptors that cause the redistribution of the charge transfer. This is also reflected in the higher quantum yields observed for compounds **35** and **34** when compared to that of **33**.

The anion binding properties of **33–35** were also investigated by UV–Vis and fluorescence titration experiments in CH<sub>2</sub>Cl<sub>2</sub>. The three compounds showed high selectivity toward F<sup>−</sup> anions, even when other competing anions, such as Cl<sup>−</sup>, Br<sup>−</sup>, I<sup>−</sup>, NO<sub>3</sub><sup>−</sup>, ClO<sub>4</sub><sup>−</sup>, and H<sub>2</sub>PO<sub>4</sub><sup>−</sup> are present. Upon increasing amounts of TBAF, the ICT absorption band of **33** centred at 389 nm showed a bathochromic shift, accompanied by a decrease in intensity. A simultaneous increase in the intensity of the band at 350 nm was also observed. In the case of **35** and **34**, adding increasing amounts of TBAF caused a decrease of the two bands centred at ~375 nm and ~262 nm. Fluorescence titrations of **33** with increasing amounts of TBAF caused a gradual shift of the emission band at 515 nm to the region at 450 nm (Fig. 15B) with a simultaneous increase in intensity. In contrast to **33**, which showed a fluorescence enhancement, the emission bands of **35** and **34** showed a gradual quench upon the addition of increasing amounts of TBAF.

A rare case of time-resolved fluorescence sensing of fluoride using the two triarylborane derivatives **36** and **37** (Fig. 16, A) was reported by Lee and co-workers [52]. Chemosensors **36** and **37** both consist of a triarylborane skeleton substituted with a triazine acceptor, linked in the *ortho* position of the phenylene ring with a carbazole (Cz) or a diphenylamine (DPA) donor unit, respectively (Fig. 16A). The interaction of **36** and **37** with fluoride anions causes a decrease of the strong bands in the range 270–350 nm, attributed to the donor-centered  $\pi - \pi^*$  transition mixed with the boron-centered  $\pi(\text{Mes}) - p_{\pi}(\text{B})$  charge-transfer transition (Fig. 16B). Chemosensors **36** and **37** show a further broad and weak absorption band at 413 nm and 451 nm, respectively, assigned to the ICT transition between D–A. In the case of **37**, the interaction with F<sup>−</sup> caused a blue-shift of this band as the consequence of disruption of the conjugation between the boron and triazine acceptor. Fluorescence titration of **36** with increasing amounts of fluoride anions showed ratiometric changes in the fluorescence upon F<sup>−</sup> binding, while **37** exhibited a turn-on fluorescence response. Both derivatives displayed thermally activated delayed fluorescence (TADF), behaving as a time-resolved turn-on fluorescence sensor. Both <sup>11</sup>B NMR and <sup>19</sup>F NMR measurements indicated that the fluoride is coordinated to the boron centre, causing a change in the coordination geometry. The response of chemosensor **37** in the presence of an excess of other anions, such as Cl<sup>−</sup>, Br<sup>−</sup>, I<sup>−</sup>, ClO<sub>4</sub><sup>−</sup>, NO<sub>3</sub><sup>−</sup>, and HSO<sub>4</sub><sup>−</sup>, was also studied. The system showed no response toward the set of anions analysed, leading to a strong turn-on fluorescence only in the presence of F<sup>−</sup>. The selective detection of F<sup>−</sup> by **37** was also tested in the presence of a competitive fluorophore (Coumarin 6) using time-resolved emission spectroscopy (TRES) with a delay of 100 ns. The results showed a complete disappearance of the signal from Coumarin 6, retaining only the long-lived fluorescence signals originating from the **37**·F<sup>−</sup> adduct.

Single-crystal X-ray diffraction performed on the fluoride adduct of **36** (**36**·F<sup>−</sup>) confirmed the formation of a tetra-coordinated boron (Fig. 16C). The crystal structure of **36** also showed that the design with D–A moieties substituted in the *ortho*- position on the phenylene ring introduces steric hindrance, promoting a D–A twisted conformation. As suggested by calculations, the D–A twisted conformation reduces the spatial overlap between the HOMO and LUMO, promoting a fast reverse intersystem crossing (RISC) process and, consequently, a TADF mechanism.

## 5. Metal-based chemosensors

Metal complexes possess a series of physical and chemical properties

suitable for the design of selective anion chemosensors. The metal center, with its positive charge, coordination number and geometry, represents a potential selective Lewis acid binding site for anionic species. Most importantly, the metal ion can confer specific optical, photochemical, magnetic or redox properties to the system [53]. Several classes of metal-based chemosensors have recently been reported. In most of these cases, the recognition process involves a variation of the optical or fluorescent properties of the metal complex due to the interaction of the anion with the metal center or other parts of the chemosensor [24,54,55]. In a few other cases, the anion promotes the displacement of either the metal ion or other species, causing an optical response [56–58].

Huang and Pierre have recently developed a family of two Fe(III) receptors (**38** and **39**) for the selective recognition of phosphate anions (Fig. 17) [59]. In the two complexes, Fe(III) is respectively coordinated by tetra- (**38**) and pentadentate (**39**) 1,2-hydroxypyridinone ligands, with the remaining open coordination site occupied by a fluorescein molecule. This has the dual function of preventing the formation of the  $\mu$ -oxo dimers and, at the same time, recognizing the target anion via indicator displacement assay (IDA). The ability of **38** and **39** to coordinate the phosphate anions and the concomitant displacement of the fluorescein moiety were investigated by ATR-IR, <sup>31</sup>P NMR, UV–Vis, and fluorescence spectroscopies. In particular, the fluorescence spectroscopy results show a 20-fold turn-on in fluorescence upon coordination of 1 equiv. of the PO<sub>4</sub><sup>3−</sup> anion to the Fe(III) centre of both **38** and **39** (Fig. 17A and B). The results suggest that in both cases, a 1:1 binding mode with equilibrium constants  $8.8 \times 10^5 \text{ M}^{-1}$  for Fe(III)·**38** and  $1.1 \times 10^6 \text{ M}^{-1}$  for Fe(III)·**39**. The two probes showed high selectivity over the most common competing anionic species, such as CO<sub>3</sub><sup>2−</sup>, NO<sub>3</sub><sup>−</sup>, SO<sub>4</sub><sup>2−</sup>, halides (F<sup>−</sup>, Cl<sup>−</sup>, Br<sup>−</sup>, and I<sup>−</sup>), and AsO<sub>4</sub><sup>3−</sup>.

A platinum-based dual-selective probe (**40**) for the recognition of cations and anions was recently developed by Yam and co-workers (Fig. 18) [60]. Probe **40** consists of a dipicolylamine (DPA)-containing alkynylplatinum(II) terpyridine complex, exhibiting a high affinity for Zn(II) (Fig. 18a). The addition of increasing amounts of Zn(OTf)<sub>2</sub> **40** shows a blue-shift of its low energy absorption band at 370–560 nm. The emission spectra show a band at approximately 600 nm attributed to the triplet metal-to-ligand charge-transfer (<sup>3</sup>MLCT) excited state. Complexation of Zn(II) by the DPA moiety of **40** forms the probe, **40**·Zn<sup>2+</sup>, which was able to recognize Na<sub>4</sub>P<sub>2</sub>O<sub>7</sub>. In the presence of increasing amounts of Na<sub>4</sub>P<sub>2</sub>O<sub>7</sub>, **40**·Zn<sup>2+</sup> shows an increase of the low-energy absorption band at 650 nm and a decrease of the band at 415 nm, with a concomitant formation of a well-defined isosbestic point at 347 nm (Fig. 18A left). After the addition of approximately 1 equiv. of Na<sub>4</sub>P<sub>2</sub>O<sub>7</sub>, the colour of the solution turns from yellow to orange (Fig. 18B). The emission spectra recorded at increasing concentrations of Na<sub>4</sub>P<sub>2</sub>O<sub>7</sub> show the appearance of a band at 770 nm, accompanied by a decrease of the <sup>3</sup>MLCT at 600 nm, suggesting the formation of aggregates (Fig. 18A right).

Molecular modelling and spectroscopic and spectrometric characterization suggest that the HP<sub>2</sub>O<sub>7</sub><sup>2−</sup> anion bridges two **40**·Zn<sup>2+</sup> units, which oligomerize via Pt···Pt and  $\pi - \pi$  stacking interactions, resulting in the formation of nanofibers.

Khatua and colleagues developed a cyclometalated Ir(III) complex of a methylene-bridged benzimidazole-substituted 1,2,3-triazole, **41** for the detection of H<sub>2</sub>P<sub>2</sub>O<sub>7</sub><sup>2−</sup> (Fig. 19) [61]. Compared to the examples above, in this case, the binding site involves the use of weaker and directional intermolecular interactions such as hydrogen bonding, making the anion binding process reversible. Probe **41** showed a high selectivity for H<sub>2</sub>P<sub>2</sub>O<sub>7</sub><sup>2−</sup> even in the presence of other competing anions, such as H<sub>2</sub>PO<sub>4</sub><sup>−</sup>, ATP, ADP, and AMP. In CH<sub>3</sub>CN **41** showed a weak emission at 483 nm and 510 nm ( $\lambda_{\text{exc}} = 370 \text{ nm}$ ;  $\phi = 0.016$ ) that increased upon titration with H<sub>2</sub>P<sub>2</sub>O<sub>7</sub><sup>2−</sup> (Fig. 19A). The results fit with a 1:1 binding model ( $K_{\text{a}} = 8.6 \times 10^7 \text{ M}^{-1}$ ). Using <sup>1</sup>H NMR titrations, it was demonstrated that the anion interacts with the benzimidazole-substituted 1,2,3-triazole ligand via a set of C–H···O, N–H···O, and

O–H...O (Fig. 19B). Interestingly, **41** also shows low cytotoxicity against HeLa cells and is suitable for intracellular pyrophosphate imaging, opening the possibility of biological applications.

Ruthenium-based complexes represent another class of metal-based systems recently investigated for the development of selective anion-sensing probes [62–66]. Mukhopadhyay and co-workers [16] reported a fluorescent Ru(II)-complex (**42**) for anion sensing and bio-imaging (Fig. 20) [67]. Probe **42** consists of Ru(II)-arene scaffold combined with a glycine derivative. The sensing ability of **42** towards different anions ( $\text{Cl}^-$ ,  $\text{Br}^-$ ,  $\text{I}^-$ ,  $\text{CO}_3^{2-}$ ,  $\text{SO}_4^{2-}$ ,  $\text{N}_3^-$ ,  $\text{NO}_2^-$ ,  $\text{SCN}^-$ ,  $\text{BPh}_4^-$ , and  $\text{S}_2\text{O}_8^{2-}$ ) has been investigated by UV-Vis and fluorescence spectroscopy in DMSO. When titrated with various anions. Compound **42** shows a red-shift of the absorption band at 330 nm only in the presence of  $\text{CO}_3^{2-}$  and  $\text{SO}_4^{2-}$  anions (Fig. 20A). Anions  $\text{CO}_3^{2-}$  and  $\text{SO}_4^{2-}$  also cause a significant quench of the fluorescence (Fig. 20B). Both anions interact with **42** in a 1:1 ratio via H-bond formation with the N–H and the adjacent aromatic C–H, with binding constants of  $K_a = 3.97 \times 10^4 \text{ M}^{-1}$  and  $2.59 \times 10^4 \text{ M}^{-1}$  for the formation of the adducts with  $\text{CO}_3^{2-}$  and  $\text{SO}_4^{2-}$ , respectively.

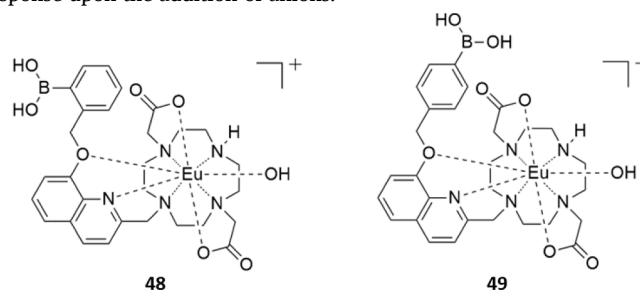
Due to their photophysical properties, such as sharp emission spectra and long luminescence life-time (up to ms), Lanthanide-based receptors represent another class of metal complexes that have received much attention in anion sensing [68]. Similar to what was observed for other metal-based receptors, anion binding and recognition processes by lanthanide-based probes can be achieved using different approaches. Lanthanide complexes, due to their affinity for oxyanions, represent the ideal candidates for the design of phosphate probes [69]. Accordingly, a number of recent examples focused on the development of probes for the detection of phosphates and nucleoside phosphate anions [70–73].

Anzenbacher and co-workers developed three carboxamidequinoline-Eu(III) complexes (**43–45**) for the recognition of phosphates in water (Fig. 21A) [74]. Upon complexation of Eu(III), the ICT state is suppressed, resulting in a quenched fluorescence emission of the carboxamidequinoline scaffold. The coordination of Eu(III) by phosphate species determines the displacement of the ligand and, consequently, the regeneration of its fluorescence emission (Fig. 21B). The three probes exhibit a higher affinity for ATP, followed by species with a decreasing number of phosphate moieties ( $\text{HP}_2\text{O}_7^{3-}$ , ADP,  $\text{H}_2\text{PO}_4^-$ , and AMP), as would be expected considering the role of electrostatic interactions in the binding process. In this sense, the selectivity of most reported nucleoside phosphate probes follows the order  $\text{ATP} > \text{ADP} > \text{AMP}$  [75]. Therefore, achieving a selectivity for dihydrogenphosphate or AMP anions in the presence of the other competing species is not straightforward.

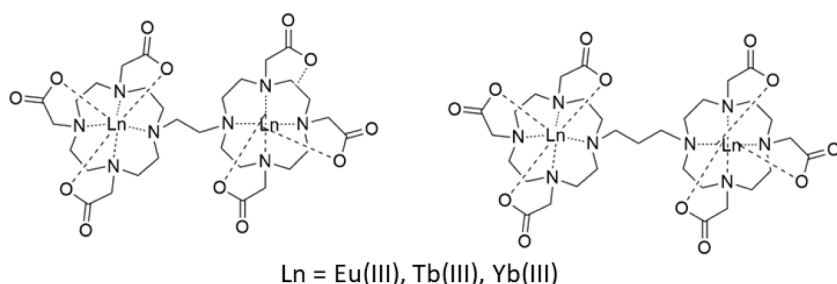
Recently, Butler and co-workers [75] have developed two macrocyclic receptors based on a cyclen scaffold, functionalized with a steric demanding 8-(benzyloxy)quinoline pendant arm able to coordinate Eu(III) (complexes **46** and **47**). The 8-(benzyloxy)quinoline pendant arms take part in coordinating the Eu(III) centre in the axial site, occupying the top of the receptor, also acting as an antenna and therefore providing an efficient sensitization of the Eu(III) emission. Furthermore, in order to achieve multi-site recognition, the 8-(benzyloxy)quinoline moiety of **47** is functionalized with a boronic acid function. This provides reversible interactions between the boronate ester and the ribose sugar of AMP,

supporting the coordination of the phosphate moiety to the Eu(III) center. Upon the addition of AMP, ADP, and ATP (10 mM HEPES at pH 7.0), both receptors showed an enhancement of the Eu(III) emission intensity more pronounced for AMP. The higher selectivity towards AMP was particularly evident for **47**, which showed a 4-fold enhancement in overall Eu(III) emission intensity (Fig. 22B–D). In both **46** and **47**, the steric hindrance generated by the quinoline moiety, combined with the high rigidity of the anion binding site, prevents efficient coordination by ATP and ADP, resulting in the selectivity order  $\text{AMP} > \text{ADP} > \text{ATP}$ , which is reversed with respect to that generally observed. The two receptors also show good selectivity for the phosphate anion and no response in the presence of  $\text{HCO}_3^-$  and lactate anions. Based on its promising binding properties, **47** was applied to detect inorganic phosphate in human serum samples and to monitor the enzymatic production of AMP in real-time.

In a second article by Butler and co-workers, the influence of the position of the phenylboronic acid group on the binding properties was investigated, comparing the behaviour of **47** with its *o*- and *p*-isomers (**48** and **49**) [76]. The results show that, like **47**, the *p*-isomer has higher selectivity to AMP over ATP, though it has a lower level of discrimination between AMP and ADP. Interestingly the *o*-isomer, due to the direct coordination of the phenylboronic acid to the Eu(III) centre, shows no response upon the addition of anions.



Although lanthanide-based receptors show a great affinity for oxyanions, the detection of other anionic species has also been investigated [77–80]. Faulkner and co-workers developed a family of binuclear lanthanide complexes able to bind chloride in aqueous solutions (**50–55**) [81]. The probes consist of two macrocyclic ligands bridged by flexible ethane (C-2) and propane (C-3) linkers and complexed by lanthanide metals (Eu(III), Tb(III), and Yb(III)), resulting in coordinatively unsaturated neutral binuclear complexes. These are pre-organized to form a pocket between the lanthanide centers able to host halide anions coordinated to the metals. The binding process has been investigated by  $^{35}\text{Cl}$  NMR at different temperatures (298 K, 304 K, 311 K, and 317 K) and via luminescence spectroscopy. The systems show a response upon the addition of  $\text{F}^-$  and  $\text{Cl}^-$  under physiological conditions and no observable changes towards competing halides, such as  $\text{Br}^-$  and  $\text{I}^-$ . Also,  $\text{Cl}^-$  binding involves chelation in the equatorial position between the metal centres. The association with  $\text{Cl}^-$  anions was also evaluated by high-resolution ESI-Mass spectrometry, supporting the formation of ternary complexes  $[\text{Ln}_2(\text{ligand})_2\text{C-2}(\text{m-Cl})]^-$  and  $[\text{Ln}_2(\text{ligand})_2\text{C-3}(\text{m-Cl})]^-$ .



Metal-organic frameworks (MOFs) represent an extensively investigated class of crystalline materials with different potential applications, such as gas storage, separation, and catalysis, to cite a few. The possibility to choose among a variety of metals and linkers and, therefore, design and tailor the porosity with specific H-bond donors and acceptors makes this class of materials extremely versatile. Several examples of MOFs which have been used for the detection of different anion species have been recently reported [72,73,77,79,80,82–86].

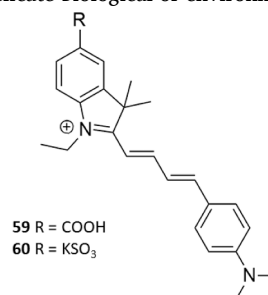
Mahata and co-workers developed a chelidamic acid - Y(III)/Mn(II) heterobimetallic MOF (**57**) for the selective detection of phosphate (Fig. 23) [87]. The system was fully characterized by single-crystal X-ray diffraction, FT-IR, UV-Vis spectroscopy, thermal gravimetric analysis (TGA), Brunauer–Emmett–Teller (BET) analysis, PXRD, and steady-state and time-resolved photoluminescence studies. Characterization by BET analysis and TGA provided information about the porosity, dehydration, and thermal stability of **57**. Structural determination by single-crystal X-ray diffraction shows the presence of hydroxyl-functionalized pockets (Fig. 23A), representing potential binding sites. Irradiation of an aqueous dispersion of **57** at 280 nm shows an emission peak at 388 nm, attributed to the intraligand transitions ( $\pi^* \rightarrow \pi$  and  $\pi^* \rightarrow n$ ). The sensing ability of **57** was investigated in the presence of different anions ( $I^-$ ,  $Cl^-$ ,  $F^-$ ,  $Br^-$ ,  $NO_3^-$ ,  $NO_2^-$ ,  $SO_4^{2-}$ ,  $C_2O_4^{2-}$ ,  $ClO_4^-$ ,  $CH_3COO^-$ , and  $PO_4^{3-}$ ). The system provided a significant response only in the presence of  $PO_4^{3-}$ , showing a 4-fold increase of the luminescent intensity (concentration up to 62.5  $\mu M$ ), with a calculated LOD of 0.2  $\mu M$  (Fig. 23, B). Furthermore, **57** proved to be highly selective for  $PO_4^{3-}$  (Fig. 23, C). The stability of **57** in aqueous media and also in the presence of  $PO_4^{3-}$  was investigated by PXRD, proving that the crystal structure remains unchanged after the detection process. The phosphate interacts with the hydroxyl-functionalized pockets, determining an enhancement of the luminescent emission.

## 6. Charged chemosensors

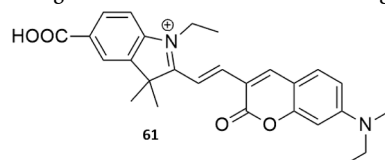
Through protein engineering, Dodani and co-workers have developed a turn-on fluorescent chloride sensor (**58**, Fig. 24) from rhodopsin GR, a light-driven proton pump derived from *Gloeobacter violaceus* [88]. To form a  $Cl^-$  binding site, the D121 position was mutated by substituting valine for aspartate, thereby changing the counterion of the phenolate chromophore. When  $Cl^-$  was added (as NaCl, 400 mM) to a system of **58** ( $\sim 3 \mu M$ ) and buffered to pH 5 with acetate and gluconate (50 and 600 mM, respectively, as NaX salts), the  $pK_a$  of the sensor shifted from  $3.1 \pm 0.1$  towards the protonated state,  $4.8 \pm 0.1$ . Under the same conditions, a pH-dependent, red-shifted fluorescent response was observed for  $Br^-$ ,  $I^-$ , and  $NO_3^-$ , while no fluorescent response was observed when  $H_2PO_4^-$  was added to the system as the NaX salts (400 mM). The dissociation constants of **58** with NaCl, NaBr, and NaI were  $K_d = 204 \pm 41$ ,  $194 \pm 14$ , and  $170 \pm 34$  mM, respectively, and interestingly, the NaCl LOD of **58** was calculated at 12.5 mM. The authors used a series of single and bulk cell *in vitro* fluorescence studies on *E. coli* expressing both the cyan fluorescent protein (CFP) and the **58** mutations, which revealed that **58** senses the changing extracellular  $Cl^-$  concentration and ruled out interference caused by perturbed membrane potential or the transmembrane ion transport facilitated by **58**. Interestingly, when **58** was encapsulated in detergent micelles under aqueous conditions, the sensor was also capable of detecting changes in the extracellular  $Cl^-$ .

Qi and co-workers have synthesised two charged chemosensors, **59** and **60**, containing a carboxyl and sulfonyl group, respectively, which are soluble in both an aqueous and cytomembrane environments [89]. Using UV-Vis studies, both **58** and **59** (10 mM) were capable of sensing  $HSO_3^-$  in water with detection limits of (4.59 and 8.19 nM, respectively) causing a colour change from blue to colourless. When added to a phosphate buffer solution (PBS) buffered to pH 7.1 containing  $HSO_3^-$ ,  $SCN^-$ ,  $N_3^-$ ,  $ClO_4^-$ ,  $HSO_4^-$ ,  $H_2PO_4^-$ ,  $AcO^-$ ,  $I^-$ ,  $Br^-$ ,  $Cl^-$ , and  $F^-$  (10  $\mu M$ , as

NaX salts), each probe (10  $\mu M$ ) only  $HSO_3^-$  elicited a significant response. The maximum fluorescence absorbance of **58** and **59** was 645 and 662 nm, respectively, while the fluorescence emission was 375 and 415 nm, respectively. The large Stokes shift of  $\sim 250$  nm was observed, effectively weakening probe auto-fluorescence and self-absorption, resulting in a heightened sensitivity to the  $HSO_3^-$  anion. The authors determined the fluorescence quantum yields of **58** and **59** to be 0.251 and 0.167, respectively. The sensing mechanism operates via the addition of  $HSO_3^-$  to the electron-deficient carbon-carbon double bond, which inhibits ICT and, subsequently, a distinct colour change from blue to colourless. The toxicity of the probes (0–10  $\mu M$ ) in B16-F10 cells showed **58** was less cytotoxic than **59**. Notably, the higher biocompatibility of **58** could lead to potential applications of this  $HSO_3^-$  sensor in delicate biological or environmental systems.



Dong and co-workers report the synthesis of a  $CN^-$  sensitive coumarin-connected carboxylic indolium near-infrared (NIR) turn-off sensor (**61**) that is both cytomembrane permeable and water-soluble [90]. The sensor was prepared in a 73 % yield following a three-step synthesis. The anion selectivity of **61** (10  $\mu M$ ) was evaluated via both UV-Vis spectrophotometry and Fluorescence studies in an aqueous solution buffered with Tris-HCl (0.01 M), adjusted to pH 7.2. The solution contained 50 equivs. of the following anions,  $SCN^-$ ,  $N_3^-$ ,  $CN^-$  (added as NaX salts) and  $ClO_4^-$ ,  $HSO_4^-$ ,  $H_2PO_4^-$ ,  $AcO^-$ ,  $I^-$ ,  $Br^-$ ,  $Cl^-$ ,  $F^-$  (added as TBA salts). Only in the presence of  $CN^-$  (with a LOD of  $4.44 \times 10^{-7}$  mol  $L^{-1}$ ) did fluorescence quenching occur. The result was an observable colour change from blue (584 nm) to colourless (425 nm) due to ITC disruption caused by  $CN^-$  addition to the  $\pi$ -conjugated indolium vinylene unit. Using the MTT assay, a B10-F10 cell viability of  $< 85$  % was achieved with **61** concentrations of 0.01–50  $\mu M$ , indicating potential use in biological or environmental  $CN^-$  sensing.

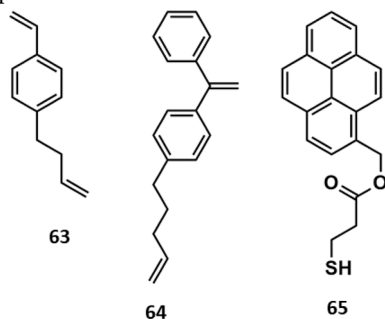


Ghosh and co-workers have reported the synthesis of **62** (Fig. 25), an Ir(III) complex functionalised with 2-phenylpyridine and 3,3'-([2,2'-bipyridine]-5,5'-diylbis(methylene))bis(1-ethyl-1H-imidazol-3-ium), in a 77 % yield [91]. Single crystal X-ray diffraction revealed **62** formed a  $2PF_6^-$  complex and maintained a distorted octahedral geometry in the solid-state (Fig. 25). PL anion competition assays, performed in  $CH_3CN$  at 298 K, showed that **62** (10  $\mu M$ ) acts as a selective lifetime-based luminescent  $H_2PO_4^-$  and  $HP_2O_7^{3-}$  (2 and 1 equiv., respectively) chemosensor in the presence of  $ClO_4^-$ ,  $I^-$ ,  $Br^-$ ,  $NO_3^-$ ,  $HCO_3^-$ ,  $Cl^-$ ,  $AcO^-$ ,  $HSO_4^-$ ,  $NO_2^-$ ,  $BzO^-$ , and  $F^-$  (10 equivs., as TBA salts). Further analysis of the PL titration data produced  $H_2PO_4^-$  ( $K_1 = 6.1 \times 10^4$  and  $K_2 = 1.1 \times 10^4 M^{-1}$ ) and  $HP_2O_7^{3-}$ , ( $K_a = 7.94 \times 10^4 M^{-1}$ ) binding constants. Interaction between **62** and  $H_2PO_4^-$  or  $HP_2O_7^{3-}$  causes a blue-shift in emission from 615 to 577 or 579 nm, respectively. A 13.7- ( $H_2PO_4^-$ ) and 8.5-fold ( $HP_2O_7^{3-}$ ) PL intensity increase was also observed alongside an increase in lifetimes ( $\tau$ ) (0.03543–0.2736 or 0.1323  $\mu s$ , respectively). Proton-NMR titrations were used to study the anion recognition mechanism of **62** (7 mM) in  $DMSO-d_6$  at 298 K and revealed hydrogen-bonding interactions between  $H_2PO_4^-$  or  $HP_2O_7^{3-}$  and the imidazolium C–H moiety.

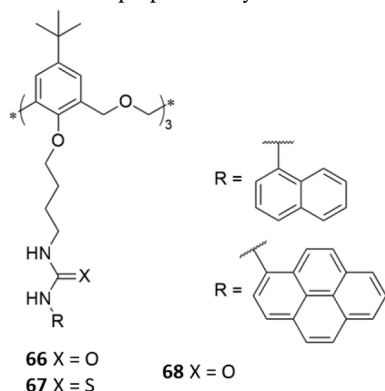
Importantly, the LOD of **62** for  $\text{H}_2\text{PO}_4^-$  and  $\text{HP}_2\text{O}_7^{3-}$  was at sub-micromolar levels and calculated to be 0.040 and 0.035  $\mu\text{M}$ , respectively.

## 7. Anion sensing using excimers

Ma and co-workers have synthesized a series of pyrene-labelled sequence-controlled polymers (SCPs) using living anionic polymerization (LAP) [92]. Three monomers, 4-(3-butenyl)styrene (**63**), 4-(5'-pentenyl)-diphenylethylene (**64**), and 3-mercaptopropanoate-oxy-methyl pyrene (**65**), were synthesized in 72, 55, and 79 % yields, respectively. The steady-state fluorescence spectrum of pyrene-labelled SCPs with average chain lengths of 0, 10, 20, 40, and 60 exhibited a near-linear relationship between monomer emission intensity (378 nm) and excimer emission intensity (481 nm). Molecular Dynamics (MD) simulations using the DPSBD method were shown to accurately describe the luminescent properties of SCPs in statistical sequences observed in experiments.

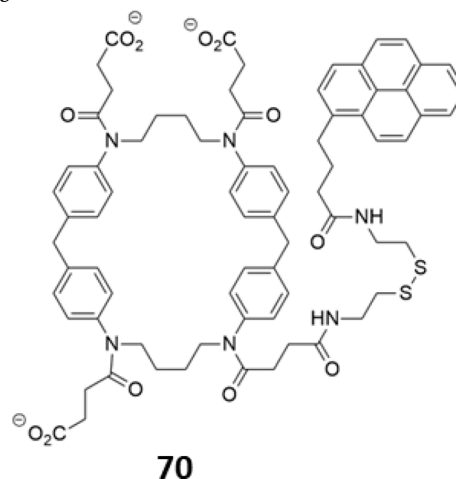


Menezes and co-workers synthesized two fluorescent naphthalene- (**66** and **67**) and pyrene-substituted (**68**) (thio)ureido-hexahomotrioxacalix[3]arene-based chemosensors in 53, 71, and 83 % yields, respectively [93]. The receptors formed 1:1 host:guest complexes via hydrogen bonds with  $\text{NO}_3^-$ ,  $\text{HSO}_4^-$ ,  $\text{ClO}_4^-$ ,  $\text{AcO}^-$ ,  $\text{BzO}^-$ ,  $\text{I}^-$ ,  $\text{Br}^-$ ,  $\text{Cl}^-$ , and  $\text{F}^-$  anions (as TBA salts) and were analyzed using  $^1\text{H}$  NMR, UV-Vis, and fluorescence titrations (0–10 equiv.). Proton-NMR titrations of **66–68** ( $2.5 \times 10^{-3}$  M) in  $\text{CDCl}_3$  at 298 K showed  $K_a$  constants increased with anion basicity with  $\text{AcO}^-$ ,  $\text{BzO}^-$ , and  $\text{F}^-$  showing the strongest binding to **68** ( $K_a = 3.42, 3.45, \text{ and } 3.31 \text{ M}^{-1}$ ). Fluorescence titrations of **68** exhibited monomer (398 nm) and excimer (498 nm) fluorescence with lifetimes of 1.98 and 25.9 ns, respectively. Using UV-Vis absorption studies in  $\text{CH}_2\text{Cl}_2$  and  $\text{CH}_3\text{CN}$ , binding constants were derived for **66–68** ( $1\text{--}2 \times 10^{-5}$  M) where, in general, the increased anion basicity of  $\text{AcO}^-$ ,  $\text{BzO}^-$ , and  $\text{F}^-$  resulted in the highest  $K_a$  values of the series. Both **66** and **68** were more efficient than the naphthyl-thiourea **67**, with thermodynamic data showing that the binding of **68** to  $\text{AcO}^-$  and  $\text{F}^-$  was driven by entropy. Computational studies using the GFN2-xTB method with ALPB, where geometry-minimized structures were further optimized using the dielectric constant of  $\text{CH}_3\text{CN}$ , showed  $\text{CH}_3\text{CN}$  molecules were directly involved in anion binding via dispersion forces or hydrogen-bonding interactions. It was also seen that the entropy and enthalpy of the system decreased proportionally with the increase in  $\text{CH}_3\text{CN}$  molecules.



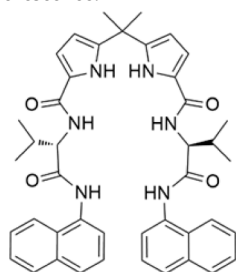
Chen and co-workers synthesized a porous hydrogen-bonded organic framework (HOF), **69**, from the hydrogen-bond driven self-assembly of 3,3',5,5'-tetrakis-(4-carboxyphenyl)-1,1'-biphenyl (Fig. 26A) [94]. Powder X-ray diffraction (PXRD) showed the three-dimensional (3D) framework was a single pure phase with a BET surface area and solvent filling space calculated to be  $2066 \text{ m}^2\text{g}^{-1}$  and 56 %, respectively (Fig. 26B). The fluorescent emission of **69** was seen to be concentration dependant with the emission of the solid (392 nm) red-shifting to 359 nm when suspended in ethanol. Further dilution decreased excimer formation and a blue-shifted emission (369–359 nm). Sensing experiments exhibited significant fluorescence quenching when  $\text{Fe}^{3+}$ ,  $\text{Cr}^{3+}$  (added as nitrate salts), and  $\text{Cr}_2\text{O}_7^{2-}$  (added as the sodium salt) ions were added to a **69** ethanol suspension and revealed  $\text{Fe}^{3+}$ ,  $\text{Cr}^{3+}$ , and  $\text{Cr}_2\text{O}_7^{2-}$  with LODs of 0.689, 2.516, and 1.638  $\mu\text{M}$ , respectively. The fluorescence resonance energy transfer and competitive absorption mechanisms account for the fluorescence quenching of  $\text{Fe}^{3+}$  and  $\text{Cr}_2\text{O}_7^{2-}$ , while the electron transfer quenching mechanism is also attributed to  $\text{Fe}^{3+}$  and  $\text{Cr}^{3+}$ . During fluorescence titrations, **69** (5 mg/100 mL) exhibited high selectivity for dopamine (10 mM) via fluorescence quenching in phosphate buffer solution with a pH range of 2–6 and revealed a LOD of 36.57 mM. Importantly, tests using fetal bovine serum biological samples containing dopamine at different concentrations showed that **69** is capable of quantitative dopamine recoveries of 101.1 % to 104.9 %.

Hayashida, Imamura, and Miyazaki have reported the synthesis and characterization of an anionic cyclophane (**70**) containing a reduction-responsive disulfide linkage and a fluorescent pyrene substituent [95]. In an aqueous polar environment containing a carbonate buffer (pH 10), self-inclusion of the pyrene moiety into the host cavity of **70** (10  $\mu\text{M}$ ) was observed with monomer emissions at 377, 398, and 420 nm. In the same system, over 30 min, the reduction and subsequent cleavage of the disulfide linkages in **70** upon contact with glutathione (GSH, 0.5 mM) generates the tetra-anionic thiolate cyclophane. The cleaved amphiphilic pyrene then self-aggregates, producing a fluorescent excimer response at 480 nm. The polarity-dependant behaviour of **70** (0.5 mM) was analyzed via  $^1\text{H}$  NMR at 298 K by altering the  $\text{D}_2\text{O}/\text{CD}_3\text{OD}$  v/v ratios from 1:9–8:2 and showed that at higher water contents, self-inclusion of the pyrene unit increased. The increased self-inclusion was accompanied by the pyrene, aromatic cyclophane, and methylene cyclophane protons shifting up-field. The authors also analyzed the concentration-dependent behaviour of **70** (0–20  $\mu\text{M}$ ) in the aqueous carbonate buffer (pH 10 at 298 K) and showed that below concentrations of  $1 \times 10^{-5}$  M, **70** exists as monomers, excimer emission at 480 nm was observed at higher concentrations.



Ghosh and co-workers have developed a fluorescent tetramide chemosensor (**71**) for  $\text{HP}_2\text{O}_7^{3-}$  using a dipyrromethene scaffold via a four-step synthesis in a 70 % yield [96]. Fluorescence studies of **71** ( $2.5 \times 10^{-5}$  M) dissolved in  $\text{CH}_3\text{CN}/\text{DMSO}$  (1 %) showed a strong excimer emission peak at 450 nm when  $\text{HP}_2\text{O}_7^{3-}$  (40 equiv., as the TBA salt) was

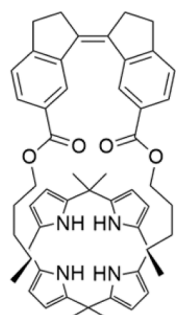
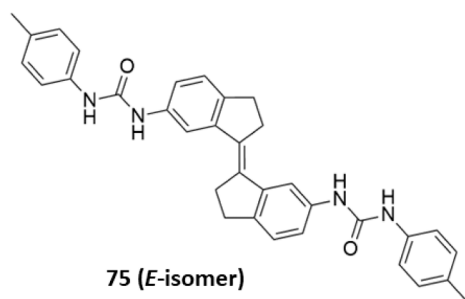
incrementally titrated to the system. However, no excimer-based fluorescence was observed upon addition of  $\text{NO}_3^-$ ,  $\text{HSO}_4^-$ ,  $\text{H}_2\text{PO}_4^-$ ,  $\text{AcO}^-$ ,  $\text{I}^-$ ,  $\text{Br}^-$ ,  $\text{Cl}^-$ , and  $\text{F}^-$  ( $1 \cdot 10^{-3}$  M, as TBA salts). From the fluorescence titrations, an  $\text{HP}_2\text{O}_7^{3-}$  binding constant of  $3.2 \times 10^3 \text{ M}^{-1}$  was found and had a detection limit of  $2.08 \times 10^{-5} \text{ M}^{-1}$ . The anion sensing ability of **71** was investigated using UV-Vis titrations in  $\text{CH}_3\text{CN}/\text{H}_2\text{O}$  (3:1, v/v) with DMSO (1 %). High selectivity for  $\text{HP}_2\text{O}_7^{3-}$  was observed, accompanied by a red-shifted emission (365–420 nm), with a binding constant and detection limit of  $4.20 \times 10^3 \text{ M}^{-1}$  and  $1.68 \times 10^{-5} \text{ M}$ , respectively. DFT studies using a 6–31G(d) basis set and a dispersion corrected B3LYP-D3 hybrid function revealed the *syn*- and *anti*-form of **71** were equilibration  $\text{CH}_3\text{CN}$ , with the low-energy *syn*-form, being preferred during  $\text{HP}_2\text{O}_7^{3-}$  binding. It was also found that anion-binding in the *syn*-form caused the naphthalene-substituents of **71** to be close, allowing  $\pi$ - $\pi$  stacking to occur, resulting in the experimentally observed enhanced excimer fluorescence.

**71**

## 8. Anion- $\pi$ interaction in sensing

George and co-workers have reported on the synthesis, characterization, and emissive charge-transfer (CT) states promoted by anion- $\pi$  interactions of a dibromo-substituted dicationic pyrometallic diimide (**72**, Fig. 27) [97]. The interaction between the **72** core and two bound  $\text{I}^-$  anions in an aqueous solution allowed ground-state CT absorption to occur, resulting in the observed CT fluorescence at 560 nm from the singlet CT state ( $^1\text{CT}$ ). Similar interactions were seen in the solid-state using single crystal X-ray diffraction, revealing both  $\text{I}^-$ - $\pi$  (Fig. 26) and  $\text{Br}^-$ - $\pi$  halogen-bonding interactions. Similarly, when supramolecular scaffolds of laponite (LP) were used to organize **72** into interlayer galleries, triplet-state phosphorescence was observed. Importantly, further steady-state and time-gated spectroscopic studies revealed the dual phosphorescence of the locally excited triplet-state ( $^3\text{LE}$ , at 470 nm) and the anion- $\pi$  triplet CT state ( $^3\text{CT}$ , at 550 nm).

Ghosh, Mondal, and Rashid have developed a Ru(II)-based chemosensor, **73**, that contains a  $\pi$ -acidic pentafluorophenyl and a halogen-bonding iodotriazole moiety as the  $2\text{PF}_6^-$  salt through a three-step synthesis in a 69 % yield (**73**• $[\text{PF}_6^-]_2$  (Fig. 28A) [40]. Single crystal X-ray diffraction revealed self-assembled polymeric chains of **73**• $[\text{H}_2\text{PO}_4^-]_2$  in the solid state due to coordination with  $\text{H}_2\text{PO}_4^-$  anions via anion- $\pi$ , halogen-bonding, and anti-electrostatic anion-anion interactions

**74 (Z-isomer)****75 (E-isomer)**

(Fig. 28A). Using DLS, transmission electron microscopy (TEM), and scanning electron microscopy (SEM) revealed polymeric structures in the presence of  $\text{H}_2\text{PO}_4^-$ . However, in the presence of  $\text{ReO}_4^-$ , supramolecular aggregation is observed, which is corroborated by dimeric solid-state structures of **73**• $[\text{ReO}_4^-]_2$  (Fig. 28C). Proton-NMR titrations in  $\text{DMSO}-d_6$  at 298 K revealed no significant interactions between **73** or  $\text{H}_2\text{PO}_4^-$  and  $\text{HP}_2\text{O}_7^{3-}$  (as TBA salts, 0–1.5 equivs.), whereas chemical shifts of  $\Delta\delta = 0.4$  and 0.6 ppm for  $\text{H}_2\text{PO}_4^-$  and  $\text{HP}_2\text{O}_7^{3-}$ , respectively, during  $^{31}\text{P}$  NMR, were indicative of phosphate-triazole halogen-bonding interactions, respectively. Similarly, up-field shifts were observed during  $^{19}\text{F}$  NMR experiments when  $\text{H}_2\text{PO}_4^-$  was added, indicative of anion- $\pi$  interactions, while no shifts were observed when either  $\text{ReO}_4^-$  or  $\text{HP}_2\text{O}_7^{3-}$  was added. Excitation of **73** at 402 and 441 nm in  $\text{CH}_3\text{CN}$  during UV-Vis studies resulted in an emission at 590 nm, corresponding to the metal-to-ligand charge-transfer (MLTC)  $^3\text{MLTC}$  luminescence band. Out of  $\text{Cl}^-$ ,  $\text{Br}^-$ ,  $\text{I}^-$ ,  $\text{HSO}_4^-$ ,  $\text{NO}_3^-$ ,  $\text{F}^-$ ,  $\text{AcO}^-$ ,  $\text{BzO}^-$ ,  $\text{HCO}_3^-$ ,  $\text{OH}^-$ ,  $\text{ReO}_4^-$ ,  $\text{HP}_2\text{O}_7^{3-}$ , and  $\text{H}_2\text{PO}_4^-$  only the addition of  $\text{H}_2\text{PO}_4^-$ ,  $\text{HP}_2\text{O}_7^{3-}$ , and  $\text{ReO}_4^-$  significantly increased emission intensity, with a 25-, 3.6-, and 1.2-fold increase, respectively. Using photoluminescence titrations in  $\text{CH}_3\text{CN}$ , the detection limits of **73** for  $\text{H}_2\text{PO}_4^-$  and  $\text{HP}_2\text{O}_7^{3-}$  were  $\sim 0.011$  and  $\sim 0.091 \mu\text{M}$ , respectively.

## 9. Photoswitchable chemosensors

The possibility of using light to change the conformation of receptors and enhance their ability to sense anions is continuing to be of great interest in supramolecular chemistry [98–102]. Wezenberg and co-workers have synthesised a photoswitchable strapped calixpyrrole (**74**), which contains a stiff-stilbene photoswitchable moiety [103]. This system, as its *Z*-isomer, can bind  $\text{Cl}^-$  anions with a remarkable 8000-fold higher affinity than the *E*-isomer ( $K_a = 1.6 \times 10^6 \text{ M}^{-1}$  and  $K_a = 2.0 \times 10^2 \text{ M}^{-1}$  for the *Z*- and *E*-isomer, respectively). Photoisomerization from *Z* to *E* can be achieved by simply irradiating a solution of the sample in DMSO or  $\text{CH}_3\text{CN}$  at 365 nm. The isomerisation results in changes in the absorbance properties of **74**, which can be reversed by irradiating at 340 nm.

Wezenberg, in collaboration with Beves, has reported that the stiff-stilbene photoswitchable compound **75** binds anti-electrostatic  $\text{H}_2\text{PO}_4^-$  oligomers via H-bonds [104]. The binding ability of **75** was studied via DOSY-NMR experiments. The diffusion rate of **75** is slower by 7 % in the *E*-isomer than in the *Z*-isomer. This is due to the fact that the *E*-isomer is more elongated. In the presence of  $\text{H}_2\text{PO}_4^-$  oligomers, which form in DMSO solution at a concentration of 50 mM, the diffusion rate of the adducts of **75** and the oligomers decreases by 33 % and 26 % for the *E*-isomer and the *Z*-isomer, respectively. This means that in the presence of the anion, there is an enhancement of the change in diffusion upon photoisomerization, opening interesting perspectives toward the directional motion of the receptor driven by light or concentration gradient.

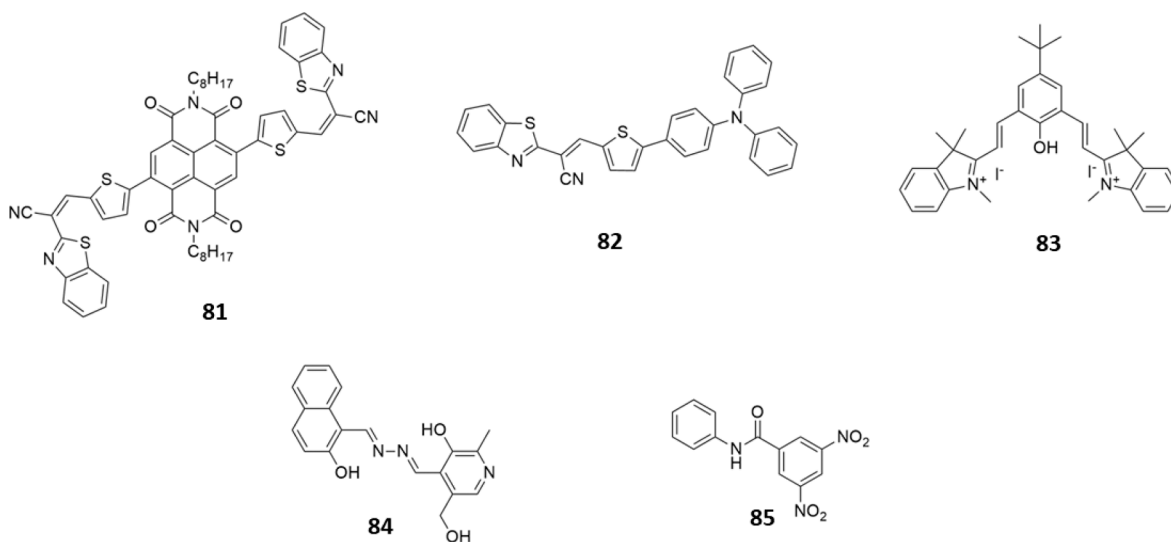
A new class of photoswitchable anion receptors containing a guanidinium moiety have been recently reported by Custelcean, Moyer and co-workers [105]. Receptor **76**, as its triflate salt, exists as either the *E,E*- or *Z,Z*-isomer, and the two can reversibly photoswitch when irradiated with a UV light (Hg vapour lamp). The *E,E*-isomer can bind  $\text{SO}_4^{2-}$  via H-bond formation and shows an affinity 5 orders of magnitude higher than that of the *Z,Z*-isomer ( $\text{Log } K_{11} = 7.25$  and  $\text{Log } K_{11} = 1.85$  for the *E,E*- and the *Z,Z*-isomer, respectively) as demonstrated by UV-Vis and  $^1\text{H}$  NMR titrations in  $\text{DMSO}-d_6$ . Receptor **76** is also able to form adducts with 1:2 stoichiometry with  $\text{SO}_4^{2-}$  when an excess of anion is present in the solution. Interestingly, the authors developed a photo-induced anion-separation process, as shown in Fig. 29. In the presence of a high concentration of  $\text{SO}_4^{2-}$  in DMSO, the adduct formed with the *E,E*-isomer immediately precipitates. However, upon irradiation (or heating), the receptor converted back to the *Z,Z*-isomer, allowing the  $\text{SO}_4^{2-}$  to redissolve.

## 10. Chemodosimeters

When a receptor reacts with a specific analyte, and the reaction causes a change in the colorimetric or fluorescence properties of the system, the sensor is referred to it as a chemodosimeter. Various examples of chemodosimeters for fluoride sensing have been recently reported [106–108].

Chemodosimeters **77–80** contain a silyl fragment which is released upon the addition of fluoride, causing dramatic changes in the fluorescent emission of the system (see Fig. 30B and C in the case of **80**). In particular, the emission band at around 380 nm ( $\lambda_{\text{exc}} = 300$  nm) of compound **80** increased in the presence of fluoride in a THF solution, but it was unaffected by other anions (Fig. 30A). The mechanism of the sensing was demonstrated by  $^1\text{H}$  NMR titrations in  $\text{CDCl}_3$  at 298 K.

A carborane-based chemodosimeter for fluoride was reported by Lee and co-workers in which the reaction triggered by fluoride is a deboronation that causes an enhancement of the fluorescence emission in a THF/ $\text{H}_2\text{O}$  (1:1, v/v) mixture [109]. Examples of chemodosimeters for  $\text{CN}^-$  sensing have also been described in the last two years, based on nucleophilic addition of cyanide to cyano vinyl moieties as in the case of compounds **81** [110] and **82** [73], nucleophilic addition to the indolynium group, as in the case of compound **83** [111], or deprotonation of the OH moiety as in the case of compound **84** [112].



Compound **85** can sense  $\text{CN}^-$  via nucleophilic aromatic substitution of three cyanide groups on the dinitrophenyl-substituted ring. In the UV-Vis spectrum of **9** in  $\text{DMSO}/\text{H}_2\text{O}$  (8:2, v/v), three bands appeared attributed to the mono, the bi-, and the tri-substituted derivative. The reaction is accompanied by a colour change of the solution from colourless to purple as well as a change in the emission properties of the system [113].

Gong, Chow, and co-workers described a novel approach in cyanide sensing and developed an interesting bimetallic system **86**, which is able to colorimetrically sense  $\text{CN}^-$  at pH 7 in phosphate buffer and then act as a catalyst to degrade it (Fig. 31) [114]. As described in Fig. 31, in compound **86**, the Fe(II)-diimine portion acts as a colorimetric indicator, and then, the Cu(II) complex is able to catalytically degrade the analyte to less toxic cyanate ( $\text{OCN}^-$ ) in the presence of  $\text{H}_2\text{O}_2$ , offering the possibility to sense and detox a  $\text{CN}^-$  contaminated samples at the same time. The system is highly selective for  $\text{CN}^-$  over other interfering anions such as  $\text{AcO}^-$ ,  $\text{SO}_4^{2-}$ ,  $\text{SCN}^-$ ,  $\text{OCN}^-$ ,  $\text{NO}_3^-$ , and  $\text{N}_3^-$ . When supported on silica-gel, the colour change was detectable by the naked eye and could degrade  $\text{CN}^-$  in real samples such as tap water, river water, and underground water with a LOD of  $1.16 \times 10^{-4}$  M.

An azulene-based chemodosimeter (**87**) for nitrite colorimetric recognition in  $\text{CH}_3\text{CN}/\text{H}_2\text{O}$  (1:1, v/v) at pH = 1 was reported by Wenk, James and Lewis (Fig. 32) [115]. The sensing mechanism is shown in Fig. 31 and consists of a diazotization of the amine moiety on the azobenzene followed by the formation of a diazoquinone (**88**, Fig. 32).

The proposed system is characterised by a high selectivity over other anions such as  $\text{Cl}^-$ ,  $\text{Br}^-$ ,  $\text{I}^-$ ,  $\text{HCO}_3^-$ ,  $\text{HSO}_3^-$ ,  $\text{PO}_4^{3-}$ ,  $\text{NO}_3^-$ , and, with respect to the standard Griess test for nitrite recognition requires only the preparation of one standard solution instead of three. Compound **87** was used to detect nitrite in cured meat, and the results obtained were comparable with those obtained using the current British Standard of testing. The LOD was  $0.23 \text{ mgL}^{-1}$ , which is below the maximum concentration allowed in drinking water ( $0.5 \text{ mgL}^{-1}$ ) in the European Community.

A turn-on chemodosimeter (**89**) for hydroxide recognition showing both a colorimetric and fluorimetric response was proposed by Mariappan and co-workers (Fig. 33, A) [116]. The anthraquinone macrocycle **89** in  $\text{CH}_3\text{CN}$  solution is able to react with 1 equiv. of TBAOH, causing the deprotonation of the macrocycle and a change in the colour of the solution, as shown in Fig. 33B. When an excess of TBAOH is present in the solution, a dramatic change in the emission